DOI: 10.1002/chem.200601529

Mixed-Metal (Platinum, Palladium), Mixed-Pyrimidine (Uracil, Cytosine) Self-Assembling Metallacalix[*n*]arenes: Dynamic Combinatorial Chemistry with Nucleobases and Metal Species

Elisa Gil Bardají,[a] Eva Freisinger,*[b] Burkhard Costisella,[a] Christoph A. Schalley,[c] Wolfgang Brüning,[a] Michal Sabat,[d] and Bernhard Lippert*[a]

Dedicated to Professor Barnett Rosenberg on the occasion of his 80th birthday

Abstract: Reactions between the mononuclear mixed-nucleobase complex $[Pt(en)(UH\text{-}N1)(CH_2\text{-}N3)]^+$ (**1**; en: ethylenediamine; UH-*N1*: uracil monoanion bonded through the N1 atom; CH_2-*N3*: neutral cytosine bonded through the N3 atom) and $[Pd^{II}(en)]$ or $[Pd^{II}(2,2'\text{-bpy})]$ (2,2′-bpy: 2,2′-bipyridine) lead to libraries of compounds of different stoichiometries and different connectivities. In these compounds, the palladium entity binds to or cross-links either the N3 sites of uracil and/or the N1 sites of cytosine, following deprotonation of these positions to give uracil dianions (U) and cytosine monoanions (CH). Cyclic species, which can be considered as metallacalix[*n*]arenes, have been detected in several cases, with *n* being 4 and 8. The complexity of the compounds formed not only results from the possibility of the two different nucleobases in building block **1** engaging in different connectivities with the Pd entities, but also from the potential for the formation of oligomers of different sizes and different conformations; in the case of cyclic tetranuclear Pt_2Pd_2 species, this can, in principle, lead to the various arrangements (cone, partial cone, 1,2-alternate, 1,3-alternate) known from calix[4]arene chemistry. A further complication arises from the fact that, depending on the mutual orientation of the exocyclic groups of the two nucleobases (O2 and O4 of uracil, O2 and N4 of cytosine), these sites can be engaged in additional chelation of $[Pd^{II}(en)]$ and $[Pd^{II}(2,2'\text{-bpy})]$. Thus, penta-, hexa-, and octanuclear complexes, Pt_2Pd_3, Pt_2Pd_4, and Pt_2Pd_6, derived from cyclic Pt_2Pd_2 tetramers have been isolated and characterized.

Keywords: combinatorial chemistry · metallacalixarenes · palladium · platinum · self-assembly

Introduction

The replacing of the methylene groups in calixarenes by square-planar metal centers and the phenol rings by substituted pyrimidines grants access to metallacalix[*n*]arenes (Scheme 1),[1] with the cyclic uracil complex $[\{Pt(en)(UH\text{-}N1,N3)\}_4]^{4+}$ (en: ethylenediamine; UH: uracil monoanion) being one representative example.[2] There is not only a close conceptual analogy between organic calixarenes and cyclic oligonuclear complexes derived from *cis*-$M^{II}a_2$ (*a*:

[a] E. Gil Bardají, Prof. Dr. B. Costisella, Dr. W. Brüning, Prof. Dr. B. Lippert
Fachbereich Chemie
Universität Dortmund
Otto-Hahn-Strasse 6, 44221 Dortmund (Germany)
Fax: (+49) 231-755-3797
E-mail: bernhard.lippert@uni-dortmund.de

[b] Dr. E. Freisinger
Institute of Inorganic Chemistry
University of Zürich
Winterthurerstrasse 190, 8057 Zürich (Switzerland)
Fax: (+41) 44-635-6802
E-mail: freisinger@aci.unizh.ch

[c] Prof. Dr. C. A. Schalley
Institut für Chemie und Biochemie—Organische Chemie
Freie Universität Berlin
Takustrasse 3, 14195 Berlin (Germany)

[d] Dr. M. Sabat
Department of Chemistry
University of Virginia
Mc Cormick Road, Charlottesville, VA 22901 (USA)

Supporting information for this article is available on the WWW under http://www.chemeurj.org/ or from the author.

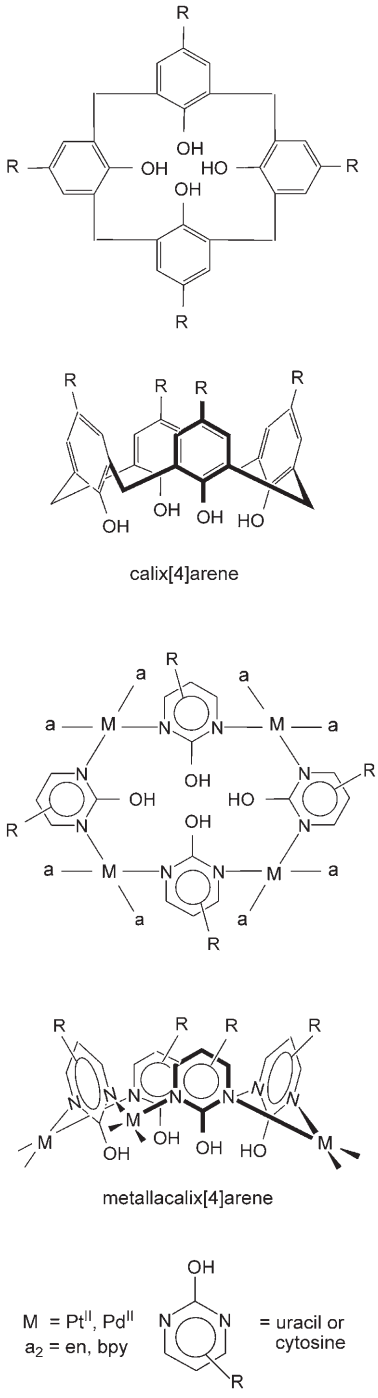

Scheme 1. Analogy between calix[4]arenes and metallacalix[4]arenes. 2,2′-bpy: 2,2′-bipyridine; en: ethylenediamine.

NH_3 or amine; a_2: diamine; M: Pt or Pd) and substituted pyrimidine ligands; more importantly, a structural and functional analogy between both types of compounds is evidenced by their capabilities to act as host compounds for guest molecules[3,4] and to permit decoration of the oxygen "rim" by additional metal ions,[5] as well as by the fact that they come in different ring sizes ranging from $n=3$[6] to $n=4$[1–4] and $n=6$.[7] As demonstrated by Navarro and co-workers, there is also the possibility to combine the pyrimidine ligand with another ditopic ligand, such as 4,7-phenanthroline.[8] Also, three-dimensional polymeric materials displaying similar structural motifs, for example, rings with four or six metal ions, have been reported, which show interesting adsorption phenomena.[9] A remarkable feature of the discrete metallacalix[*n*]arenes derived from the pyrimidine nucleobases uracil or thymine is their propensity to add additional square-planar *cis*-Ma_2^{II} (M: Pt, Pd) or *cis*-octahedral metal entities (Ni^{II}, Cu^{II}) to yield higher nuclearity species. Octanuclear compounds have been derived from Pt–calix[4]arenes[5a,10] and pentanuclear species from either Pt–calix[4]arenes[4,5c] or Pt–calix[3]arenes.[11,12] These findings are in a way reminiscent of observations with other Pt complexes containing model nucleobases, such as 1-methyluracil, 1-methylthymine, 1-methylcytosine, or 9-alkylpurines, for which we have systematically studied the formation of multinuclear derivatives.[13] Besides the interesting structural features of these supramolecular complexes, their solution chemistry may contribute to a more comprehensive understanding of the solution chemistry of the so-called "platinum pyrimidine blues", a class of Pt antitumor agents once considered very promising.[14] While there is a reasonably good understanding of the mixed valency of these compounds derived essentially from "blues" containing related ligands,[15] the complexity of the *cis*-$Pt^{II}(NH_3)_2$–uracil system[16] is still unsolved.

Here, we present evidence for the formation of mixed-metal (Pt, Pd), mixed-amine macrocycles containing two different pyrimidine nucleobases, namely unsubstituted cytosine and unsubstituted uracil (Scheme 2). By starting with $[Pt(en)(UH\text{-}N1)(CH_2\text{-}N3)]^+$ (**1**; CH_2: neutral cytosine) and treating this compound with either $[Pd^{II}(2,2'\text{-bpy})]$ (2,2′-bpy: 2,2′-bipyridine) or $[Pd^{II}(en)]$, we were able to isolate the unprecedented metallacalix[8]arene and, in particular, a series of multinuclear derivatives of two different metallacalix[4]arenes.

While the Pt–N bonds are kinetically robust, the Pd–N and Pd–O bonds are (more) labile. The formation of mixed-

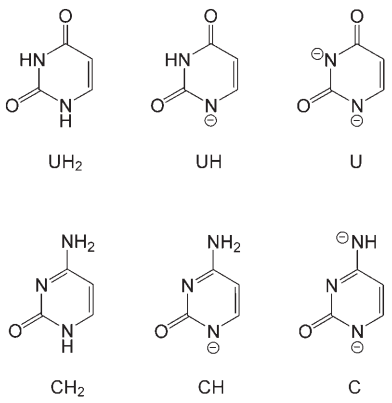

Scheme 2. Structures and abbreviations used for uracil and cytosine ligands. For UH, only the N1 deprotonated tautomer is shown, and likewise other mesomeric structures are ignored.

metal metallacalix[*n*]arenes is thus reversible and proceeds under thermodynamic control. Consequently, they might be adequately discussed in terms of the concept of dynamic combinatorial chemistry (DCC).[17] Fortunately, some of the products formed were sufficiently stable to allow isolation and kept their integrity when redissolved in water so that they could be adequately characterized.

Results and Discussion

Structure of the starting compound [Pt(en)(UH-*N1*)(CH_2-*N3*)]X·*n*H_2O (1): Reaction of [Pt(en)(UH-*N1*)Cl] with AgX and unsubstituted cytosine (CH_2) gave [Pt(en)(UH-*N1*)-(CH_2-*N3*)]X·*n*H_2O (X = NO_3, *n* = 3.5 (**1a**); X = ClO_4, *n* = 3 (**1b**)). The X-ray crystal structure of **1a** is reported here. Compound **1a** (Figure 1) crystallizes with two crystallographically different cations. Pt binding is through the N1 atom of the uracilate ligand and through the N3 atom of the cytosine. If the O2 groups of two nucleobases are used as a reference, the bases are oriented *head–tail* in both cations. The two cations in **1a** differ with regard to the angles between the nucleobases and between the nucleobases and the PtN_4 planes (**1a** I and II), respectively. In addition, the puckers of the en ligands are different in **1a** I and II. The dihedral angles with the metal planes likewise differ, for example, 79.5(3)° (CH_2) and 75.2(2)° (UH) in **1a** I and 87.8(2)° (CH_2) and 80.7(2)° (UH) in **1a** II. The internucleobase angles are 77.8(2)° in **1a** I and 78.1(2)° in **1a** II. The distances and angles about the Pt and within the ligands are not unexpected (see the Supporting Information). The differences between coordinated and free ligands (CH_2,[18a] UH_2[18b]) follow expectations previously discussed in detail for related coordination patterns.[1,19,20] In the perchlorate salt **1b**,[21] the two bases likewise adopt a *head–tail* orientation and hence the O2 atom of the uracilato ligand and the O2 atom of the cytosine reside on different sides of the Pt coordination plane. Both cation I of **1a** and cation **1b** form centrosymmetric dimers which are hydrogen bonded through the N3–H and O4 sites of the uracilato ligands (2.81(1) Å in **1a**, and 2.85(1) Å in **1b**; see the Supporting Information). Similar self-pairing schemes have been observed in other metal complexes containing N1-bonded pyrimidine nucleobases.[22] The cytosine ligands of cation II of **1a** also form centrosymmetric pairs, through the N1–H and O2 sites, with the hydrogen bonds being 2.813(9) Å in length (see the Supporting Information). The water molecules and the anions are involved in numerous hydrogen-bonding interactions as well.

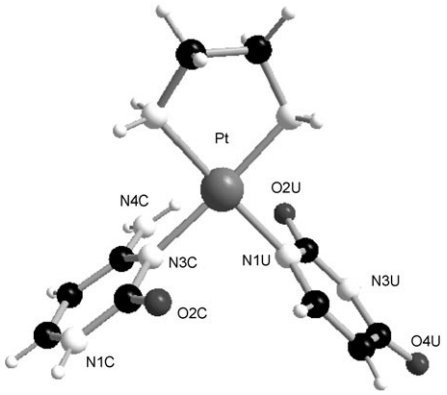

Figure 1. View of one of the two crystallographically different cations of compound [Pt(en)(UH-*N1*)(CH_2-*N3*)]NO_3·3.5H_2O (**1a**) with the atom-numbering scheme. Cation I is shown; the other one (cation II) is very similar.

^{1}H NMR spectra of 1: The ^{1}H NMR spectra of **1** in D_2O consist of discrete doublets ($^3J \approx 7.1$ Hz for both nucleobases) for the H5 and H6 resonances. Only single sets of proton signals for the individual bases are observed, a result suggesting either rapid rotation of the nucleobases on the NMR timescale or hindered rotation. The chemical shifts are listed in Table 1. The assignment of the resonances to the individual bases was accomplished by means of a ^{195}Pt edited spectrum (see the Supporting Information). According to this spectrum, the cytosine displays ^4J coupling between ^{195}Pt and H5 (17.5 Hz), whereas there is no ^5J coupling with the H6 atom. The coupling constant for the H5 atom is in the expected range.[20c] On the other hand, the H6 atom of the uracilato ligand is recognized by its considerably larger $^3J(^{195}Pt–^1H)$ coupling constant of 34 Hz, which is a consequence of the close proximity of Pt to the N1 and H6 atoms. ^4J coupling with the H5 atom of UH is not observed. For the methylene protons of the en ligand, the ^3J value is ≈42 Hz. In addition, in [D6]DMSO, NH and NH_2 proton resonances are observed, as is NH–CH coupling for several of the resonances, for example, ^3J(N1–H,H6) = 5.6 Hz for the cytosine ligand. The two protons of the N4–H_2 group of cytosine are not equivalent and give rise to two signals at $\delta = 8.36$ and 8.65 ppm. This is consistent with a slowed-down rotation of the amino group about the C4–N4 bond.

Table 1. ^{1}H NMR spectroscopic resonances (δ [ppm], in D_2O) of aromatic nucleobase protons of **1** and adducts of **1** with [Pd^{II}(2,2′-bpy)] and [Pd^{II}(en)].[a,b]

	H6 (U)	H6 (C)	H5 (C)	H5 (U)	Others	pD
1	7.59	7.51	6.02	5.61	2.73 (en)	5.45
2a	6.82	8.00	6.11	5.16	2.6–2.8 (en)	
					8.42–7.60 (bpy)	8.55
X[c]	7.62	7.86	5.90	5.51	2.68 (en)	
					8.41–7.54 (bpy)	7.51
4	7.50	7.97	6.16	5.70	2.70–2.73 (en)	
					8.43–7.15 (bpy)	9.23
7	7.81	8.26	6.33	6.07	2.70–2.73 (en)	
					8.42–7.16 (bpy)	4.45
Y[d]	6.73	7.81	5.94	5.00	2.80–2.69 (en)	7.68
10′	7.17	7.67	5.83	5.35	2.5–3.0 (en)	4.65
11′	7.36	7.90	5.66	5.62	2.5–3.2 (en)	5.32

[a] No differentiation of protonation state for uracil (U) or cytosine (C) has been considered. [b] ^3J coupling constants for H5 and H6 resonances were approximately 6.8–7.3 Hz. [c] **X**: **5a**, **5b**, or **6**. [d] **Y**: **3′** or **6′**.

Resonances of **1** in D_2O are constant over a wide range of pH* values (1.5–8.5; pH*: uncorrected pH meter reading). In more strongly alkaline solution, deprotonation of the cytosine N1−H position takes place ($pK_{a1} \approx 9.9$) and deprotonation of the uracilato ligand at N3−H eventually also occurs ($pK_{a2} \approx 11.4$). While the uracil H5 and H6 signals and the cytosine H5 signal are shifted upfield as a consequence of deprotonation, the cytosine H6 signal undergoes a downfield shift (see the Supporting Information). The acidifications of the two nucleobases as a consequence of Pt^{II} binding are thus from $pK_a = 12.15$[23] to ≈ 9.9 for cytosine, hence 2.25 log units, and from 13.5–14.2 (pK_{a2} of uracil)[24] to ≈ 11.4 for uracil.

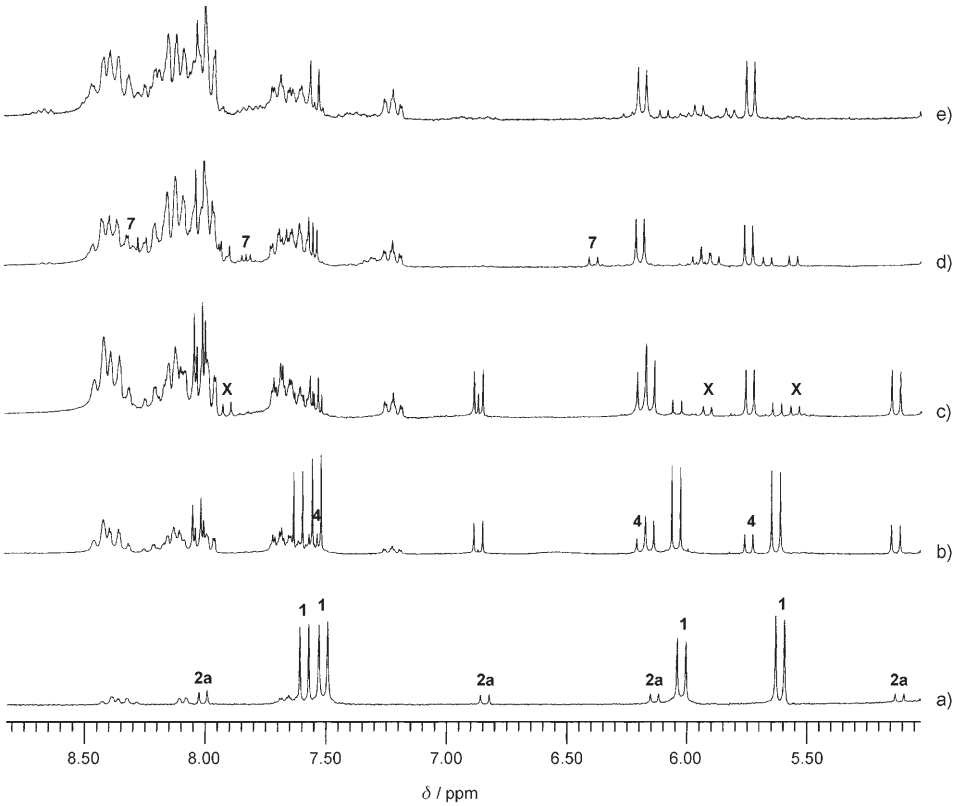

Figure 2. Low-field sections of the ^1H NMR spectra of reaction mixtures of **1a** with $[Pd(2,2'\text{-bpy})(D_2O)_2]^{2+}$ in D_2O at 20 °C with different ratios r(Pt:Pd) between the two components: a) $r = 0.1$, b) $r = 0.5$, c) $r = 1$, d) $r = 2$, and e) $r = 3$. pD values of the samples were approximately 7–7.5. For assignment of individual nucleobase resonances see Table 1. Resonances **X** refer to a complex of unknown composition, possibly **6** (or **5a** or **5b**).

Reactions of 1a (1b) with $[Pt^{II}(en)]$: Addition of $[Pt(en)(D_2O)_2]^{2+}$ (1:1) to solutions of **1a** (**1b**) in D_2O at 40 °C was followed by ^1H NMR spectroscopy. Within hours after the start, marked changes took place, which included a rapid drop in the pH* value (from approximately 5 to about 2), development of a yellow color, loss of the H5 doublets of both nucleobases (uracil, cytosine) of **1a** (**1b**) due to isotopic exchange, and formation of numerous (>10) H6 singlet resonances spanning the chemical shift range of approximately $\delta = 6.8$–7.8 ppm, after addition of NaOD to reach pH* ≈ 5. Although these observations could not be interpreted in any straightforward way, the drop in pH* value and the marked upfield shift of the H6 resonances in comparison to those of **1a** (**1b**) were attributed to reactions which involved deprotonation of one or both nucleobases as a consequence of additional Pt^{II} coordination.

Reactions of 1a (1b) with *cis*-$Pd^{II}a_2$: Owing to the failure to characterize any of the products formed from **1a** (**1b**) with $[Pt^{II}(en)]$, we resorted to experiments in which **1a** (**1b**) was allowed to react with $[Pd^{II}(en)]$ or $[Pd^{II}(2,2'\text{-bpy})]$. The major difference with the Pd species in comparison to the results with $[Pt^{II}(en)]$ was the sharpness of the resonances observed in the ^1H NMR spectra in the mixed-metal systems. Representative spectra obtained upon mixing **1a** (**1b**) and $[Pd^{II}(2,2'\text{-bpy})]$ or $[Pd^{II}(en)]$, respectively, at different ratios and at moderately alkaline pH values are given in Figures 2 and 3. There are two general points to be noted. First, some of the spectra display a large number (10 or more) of doublets for the H5 and H6 nucleobase resonances, a result indicating a multitude of species being formed simultaneously. Second, a gradual isotopic exchange of the H5 resonances of the uracil (and to some extent also of the cytosine) ligands is frequently observed; this exchange results in "pseudotriplet" patterns of H6 resonances or eventually in H6 singlets (see, for example, the resonance at $\delta \approx 6.8$ ppm in spectrum c of Figure 2).

In spectra containing $[Pd^{II}(2,2'\text{-bpy})]$, severe overlap of the bipyridine resonances occurs and this also affects the H6 nucleobase resonances. With few exceptions, these resonances were not analyzed for this reason. On the other hand, with samples isolated and redissolved in D_2O, the relative intensities of the nucleobase H5 resonances and the 2,2′-bpy resonances permitted determination of the Pt:Pd stoichiometry.

In the following sections, isolated and structurally characterized products obtained from reactions of **1a** (**1b**) and $[Pd^{II}(2,2'\text{-bpy})]$ will be discussed, followed by products derived from **1a** (**1b**) and $[Pd^{II}(en)]$. Based on these established structures, the possible ways of formation will be discussed, including those for species that have not explicitly been detected by ^1H NMR spectroscopy.

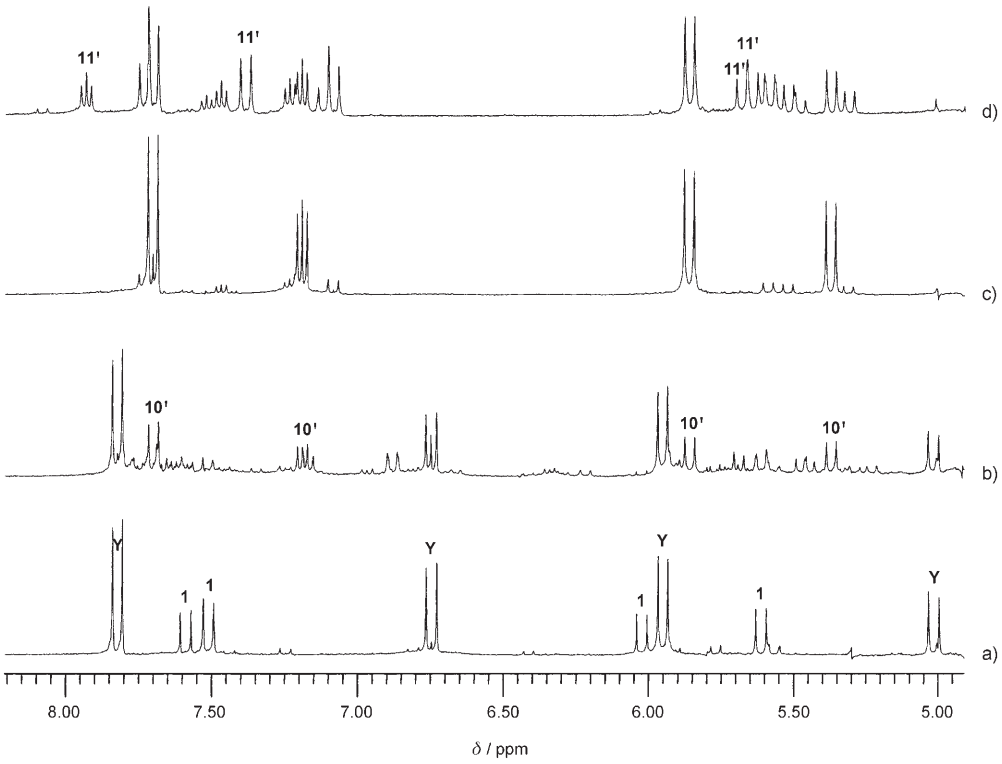

Figure 3. Low-field sections of the ^{1}H NMR spectra of mixtures obtained from **1a** and $[Pd(en)(D_2O)]^{2+}$ in D_2O at 20 °C with different ratios r(Pt:Pd): a) $r=0.5$, b) $r=1$, c) $r=2$, and d) $r=3$. pD values of the samples were approximately 7–7.5. For assignment of cytosine and uracil resonances, see Table 1. Resonances **Y** refer to a Pt_2Pd_2 complex, presumably **3′** (see the text for further details).

Isolated species from 1a (1b) and [Pd^{II}(2,2′-bpy)] with uracil, cytosine, cytosine, uracil connectivity: **Pt$_2$Pd complex 2a**: Addition of [Pd^{II}(2,2′-bpy)] to an aqueous solution of **1a** (**1b**) in a ratio of $r=0.1$ (Figure 2, spectrum a) leads to the appearance of resonances for a new species, which we were able to isolate and characterize as the Pt_2Pd complex $[(2,2'\text{-bpy})Pd\{(N1\text{-CH-}N3)Pt(UH\text{-}N1)\}_2]^{2+}$ (**2a**). **2a** was obtained as the mixed ClO_4^-, NO_3^- salt. It crystallizes as two crystallographically independent cations, which are, however, structurally very similar. Two views of one of the cations of **2a** are given in Figure 4. Selected structural features are compiled in Table 2 as well as in the Supporting Information. The formation of **2a** is the result of two cations of **1** being cross-linked by a [Pd^{II}(2,2′-bpy)] entity through the N1 positions of the cytosine ligands, after deprotonation of these sites. Preferential binding of Pd^{II} to the N1 site of cytosine as opposed to the N3 position of uracilate may be expected, given the lower pK_a value for the N1–H bond of cytosine (see above). However, when the binding patterns seen in other structurally characterized compounds containing Pd–uracil-*N3* bonds are taken into consideration (see below), this argument should not be overemphasized. After all, the reactive Pd "aqua" species is present largely as a hydroxo complex capable of abstracting weakly acidic protons from nucleobases. As a consequence of this cross-linking pattern, the sequence of nucleobases in the open tetrakis(nucleobase) complex **2a** is [(UH-*N1*)Pt(*N3*-CH-*N1*)Pd(*N1*-CH-*N3*)Pt(*N1*-UH)]; hence, the two inner cytosine nucleobases are adjacent to each other. They are oriented *head–tail*, thereby causing the two Pt atoms to be on opposite sides of the PdN_4 coordination plane. As can be seen from Figure 4, the two terminal uracilato ligands are stacked (4.0–4.6 Å). This feature also appears to be maintained in aqueous solution, if the remarkable upfield shift of the uracil H6 resonance at $\delta \approx 6.82$ ppm and the uracil H5 resonance at $\delta \approx 5.16$ ppm as compared to **1** (Table 1) are considered. As a warning, it should be noted, however, that a simplistic comparison of nucleobase proton shifts in the various metallcalix[*n*]arenes as listed in Table 1 is problematic given the influence of numerous other factors, such as the number of metal ions bonded to a particular base, nucleobase protonation state, connectivity, or conformation.

Attempts to prepare Pt$_2$Pd$_2$ (3): Having isolated the Pt_2Pd species **2a**, we considered the possibility of also preparing the cyclic Pt_2Pd_2 species **3** by adding $[Pd(2,2'\text{-bpy})(D_2O)_2]^{2+}$ to a solution of **2a**. Although formation of a new compound was indeed detected by ^{1}H NMR spectroscopy, the compound isolated eventually proved to be of Pt_2Pd_3 stoichiometry (complex **4**). The fact that **3** was not detected on the way from **2a** to **4** does not necessarily rule out its existence, but it simply implies that it is not a major component in the solution under the conditions of the experiment.

Isolated species from 1 and [Pd^{II}(2,2′-bpy)] with uracil, cytosine, cytosine, uracil connectivity: **Pt$_2$Pd$_3$ complex 4**: If the

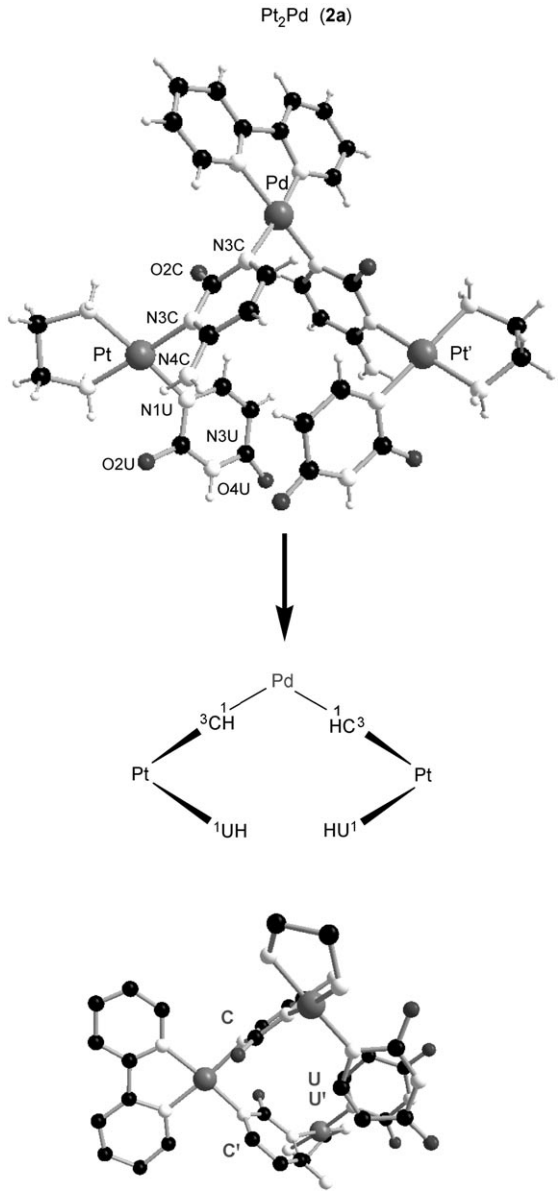

Figure 4. Different views of one of two crystallographically independent cations of $[(2,2'\text{-bpy})Pd\{(N1\text{-CH-}N3)Pt(UH\text{-}N1)\}_2](NO_3)(ClO_4)\cdot 4.9H_2O$ (**2a**).

Table 2. Selected interatomic distances [Å] and angles [°] in **2a**.[a]

Pt–N1 (U)	2.009(14)–2.026(13)	N11-Pt-N12	82.2(5)–85.8(8)
Pt–N3 (C)	1.994(11)–2.035(13)	N1 (U)-Pt-N3 (C)	87.8(5)–91.3(5)
Pt–N11	2.019(12)–2.045(14)	N11-Pt-N1 (U)	92.7(6)–94.6(6)
Pt–N12	1.930(14)–2.050(13)	N12-Pt-N3 (C)	90.2(5)–96.4(5)
Pd–N1 (C)	1.989(13), 2.024(13)	N11′-Pd-N12′	80.4(6), 81.4(6)
Pd–N1 (C′)	1.990(12), 2.033(12)	N1 (C)-Pd-N1 (C′)	88.3(5), 89.0(5)
Pd–N11′	2.000(13), 2.004(14)	N11′-Pd-N1 (C)	95.1(6), 95.8(5)
Pd–N12′	2.020(14), 2.024(14)	N12′-Pd-N1 (C′)	94.6(5), 95.4(5)

[a] For the two crystallographically independent cations, maximum and minimum values are given.

ratio of $[Pd^{II}(2,2'\text{-bpy})]$:**1** is increased (Figure 2, spectrum b), a second set of resonances appears in the ^1H NMR spectrum which, from comparison with the isolated and structurally characterized complex, is attributed to the Pt_2Pd_3 species $[\{Pd(2,2'\text{-bpy})\}_3\{Pt(en)(U\text{-}N1,N3,O4)(CH\text{-}N1,N3)\}_2]^{4+}$ (**4**). It was isolated as a nitrate salt. Figure 5 provides two different views and a schematic representation of the connectivities present in **4**. Selected structural features are listed in Table 3. The cation is cyclic, derived from **2a** by addition of two more $[Pd^{II}(2,2'\text{-bpy})]$ moieties to the uracil rings. Binding of the Pd ions is through the N3 and O4 atoms of each of the uracilate dianions; the two uracil units are again oriented *head–tail*. It can be described as an extended metallacalix[4]arene with an additional metal added to one of the

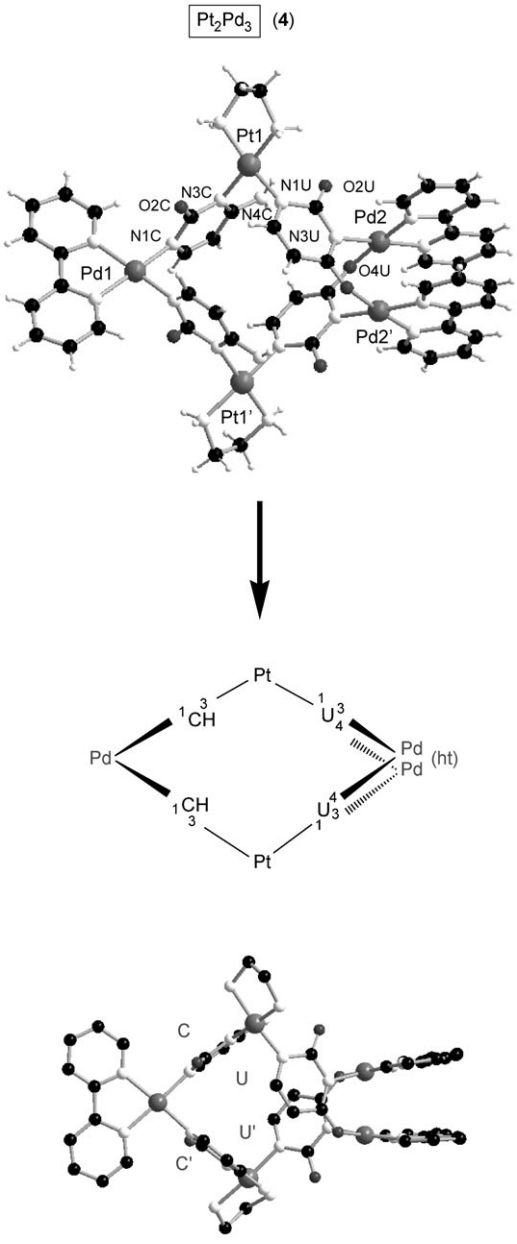

Figure 5. Two different views of the Pt_2Pd_3 cation $[\{Pd(2,2'\text{-bpy})\}_3\{Pt(en)(U\text{-}N1,N3,O4)(CH\text{-}N1,N3)\}_2]^{4+}$ (**4**) and a schematic representation of the nucleobase connectivities in **4**.

Table 3. Selected interatomic distances [Å] and angles [°] in **4**.

Pt1–N1 (U)	1.999(12)	N11-Pt1-N12	83.1(4)
Pt1–N3 (C)	2.050(11)	N1 (U)-Pt1-N3 (C)	89.3(4)
Pt1–N11	2.025(12)	N11-Pt1-N1 (U)	92.2(4)
Pt1–N12	2.046(11)	N12-Pt1-N3 (C)	96.1(4)
Pd1–N1 (C)	2.004(11)	N11′-Pd1-N12′	81.0(5)
Pd1–N1 (C′)	2.011(11)	N1 (C)-Pd1-N1 (C′)	88.1(5)
Pd1–N11′	2.016(11)	N11′-Pd1-N1 (C)	95.6(5)
Pd1–N12′	2.014(12)	N12′-Pd1-N1 (C′)	95.5(5)
Pd2–N3 (U)	1.998(10)	N11″-Pd2-N12″	80.6(4)
Pd2–O4 (U′)	2.036(8)	N3 (U)-Pd2-O4 (U′)	88.0(4)
Pd2–N11″	1.993(10)	N11″-Pd2-N3 (U)	96.6(4)
Pd2–N12″	1.989(11)	N12″-Pd2-O4 (U′)	94.8(4)
Pd2···Pd2′	2.8190(18)		

four corners. As in the precursor **2a**, the sequence of the four nucleobases is uracil, cytosine, cytosine, uracil. The four bases adopt a 1,3-alternate conformation with the reference atoms again being the exocyclic O2 groups. One of the metal corners, the one with the two adjacent uracil rings, has opened and has been replaced by a two-metal unit (Pd2, Pd2′). As a consequence of this change in the basic metallacalix[4]arene structure, some of the metal–metal distances between the metal corners are longer than the typical 5.8–5.9 Å seen in metallacalix[4]arenes. The Pd2···Pd2′ distance of 2.819(2) Å within the dimer entity of **4** is closely similar to that observed in a related dinuclear [Pd^{II}(2,2′-bpy)] complex with two bridging (*head–tail*) 1-methylthyminato ligands and N3, O4 coordination.[25]

Possible ways of formation of 4: Formation of **4** could conceivably take place from the "open" complex **2a** upon addition of two [Pd^{II}(2,2′-bpy)] entities to the N3 sites of the terminal uracilate ligands (intermediate **4a**) or alternatively to the O4 sites of the uracilate ligands (intermediate **4b**), followed by *head–tail* ring closure in both cases. As yet another alternative, a stepwise addition of [Pd^{II}(2,2′-bpy)] to **2a** with formation of the closed intermediate **3** is feasible (Figure 6). The latter pathway would involve initial formation of a Pt_2Pd_3 species in which one Pd is bonded to the two U ligands through the N3 sites (compound **3**), while the additional [Pd^{II}(2,2′-bpy)] is bonded to either the O4 atom of one uracil or the O2 of the other uracil or chelated simultaneously to both sites. Favorable stacking with the N3-bonded [Pd^{II}(2,2′-bpy)] entity could facilitate such an anchoring process of the second Pd. As the two uracils are already in a *head–tail* arrangement (1,3-alternate), a rather minor change would be necessary to generate **4**, namely a switch of one of the initial Pd–N3 bonds to a Pd–O4 bond and binding of the second Pd moiety to the now available N3 position. No nucleobase rotation would be required to accomplish this process. As mentioned above, ^{1}H NMR spectroscopy does not provide any evidence for an intermediate (**3**, **4a**, or **4b**) on the way from **2a** to **4**. Still, a comparison of the structure of the cations of **2a** and **4** reveals the relatively minor overall structural changes necessary to accomplish "addition" of two [Pd^{II}(2,2′-bpy)] to the uracil ligands (see the Supporting Information). The major structural change in going from **2a** to **4** is the loss of uracil stacking.

^{1}H NMR spectra of 4: The assignment of the ^{1}H NMR resonances of **4** with its two sets of uracil and cytosine resonances was achieved by a combination of a 2D ^{1}H,^{1}H-NOESY and 2D ^{1}H,^{13}C-COSY experiments (see the Supporting Information), as well as with the help of direct and long-range ^{1}H,^{13}C-coupling values. In the first step, a 2D ^{1}H,^{1}H-NOESY experiment was carried out. The signal of the H5 proton at $\delta = 5.70$ ppm gave intense cross-peaks to the signal of the H6 proton located at $\delta = 7.50$ ppm. Intensive cross-peaks between a second set of H5 and H6 ($\delta = 6.16$ and 7.97 ppm, respectively) resonances were also observed. An additional

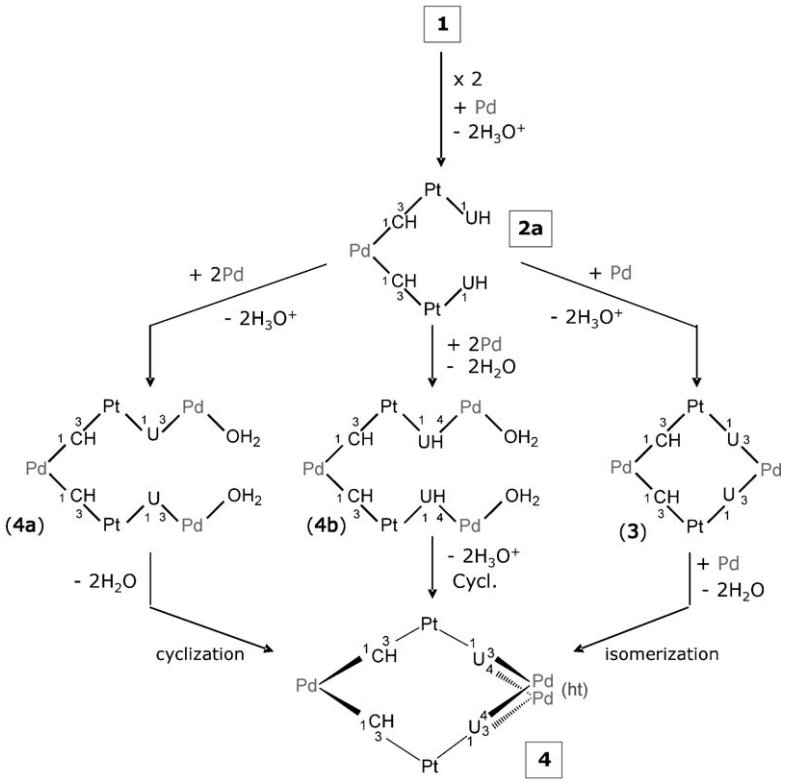

Figure 6. Possible pathways from **2a** to **4** involving closed (**3**) or open (**4a**, **4b**) intermediates.

2D experiment ($^{1}H,^{13}C$ COSY) was carried out to assign the uracil and the cytosine resonances. In the case of uracil, the signal of the H5 proton at $\delta = 5.70$ ppm gave cross-peaks to the C5 and C6 signals. The H6 resonances of uracil at $\delta =$ 7.50 ppm showed cross-peaks to the C2, C4, C5, and C6 signals, which were assigned according to reference [26]. Analogously, in the case of cytosine, cross-peaks between the signal of H5 ($\delta = 6.16$ ppm) and the C4, C5, and C6 signals were observed. Cross-peaks between the H6 resonance of cytosine ($\delta = 7.97$ ppm) and the C2, C4, C5, and C6 signals were also observed. The results of this assignment clearly showed that the upfield shift of the uracil resonances, as observed in **2a** and attributed to stacking of the uracil ligands (see above), was absent in **4a**, a result consistent with the X-ray crystal structure data.

An interesting detail in the ^{1}H NMR spectrum of **4** in D_2O is the remarkable upfield shift of one of the 2,2′-bpy resonances, namely, the triplet at $\delta =$ 7.19 ppm. In order to assign this resonance, we analyzed the 2,2′-bpy resonances of this compound in more detail, by applying ^{1}D TOCSY experiments (see the Supporting Information). The expected 12 sets of bpy resonances can be differentiated this way (that is, four sets for the 2,2′-bpy ring symmetrically bonded to Pd1 and *trans* to the cytosine N1 sites; two lots of four sets for the two stacked bpy rings, due to the nonequivalence of the two pyridine "halves" as a consequence of the different *trans*-positioned Pd2 donor atoms (on the N3 and O4 of the uracil)). The four sets of resonances for the 2,2′-bpy ligand bonded to Pd1 have chemical shifts of $\delta = 7.65$ (t), 8.09 (d), 8.33 (t), and 8.40 ppm (d). Their positions agree well with those of the bpy ligand in **2a**, as expected. The two other sets of four 2,2′-bpy resonances, representing the stacked bpy entities at Pd2 and Pd2′, are grouped at $\delta = 7.19$ (t), 7.96 (d), 8.03 (d), and 8.11 ppm (t) and at $\delta = 7.57$ (t), 7.92 (d), 7.94 (d), and 8.17 ppm (t), respectively. As pointed out, the signal at $\delta = 7.19$ ppm exhibits the highest upfield shift of all 12 of the bpy resonances, clearly reflecting bpy stacking. A view along the Pd2···Pd2′ vector in **4** allows the tentative suggestion that it is the H5 protons of the pyridine rings *trans* to the N3 positions of the uracil ligands that are located above/below the π-electron system of the pyridine half of 2,2′-bpy *trans* to the O4 positions; it is these protons that are therefore expected to experience the ring-current effect most (see the Supporting Information).

Mass spectrometry of 4: In electrospray-ionization Fourier transform ion-cyclotron-resonance (ESI-FTICR) mass spectrometry experiments, **4** could easily be ionized by stripping off the nitrate counterions to yield the +2, +3, and +4 charge states at m/z: 931.07, 600.04, and 434.53, respectively (Figure 7). From the +2 and +3 charge states, which still carry two and one nitrate counterions, respectively, the loss of HNO_3 is observed, a result indicating deprotonation of the ethylenediamine ligands at the Pt centers, as observed earlier for other similar coordination compounds.[27] Fragmentation of the parent ions occurs to some extent but does not give rise to major signals in the mass spectrum. A low-intensity signal also appears for a triply charged dimer. Analogous dimers have been observed before for other metallosupramolecular complexes[28] and are probably due to unspecific aggregation during the electrospray process.

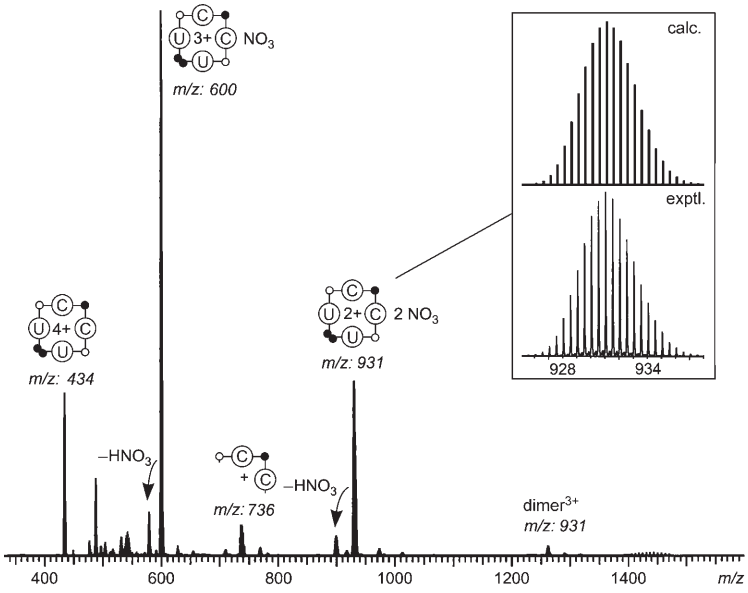

Figure 7. ESI-FTICR mass spectrum of a 150 μM solution of **4** in methanol/water (approximately 1:1). Signal assignment is indicated by the graphics (Pt: open circles; Pd: filled circles, doubly Pd-bridged corners: pair of filled circles). The inset shows the calculated (top) and experimental (bottom) isotope patterns for the doubly charged $[\mathbf{4}-2NO_3]^{2+}$ ion, which is not superimposed by a smaller fragment.

Infrared multiphoton dissociation (IRMPD) experiments were carried out with mass-selected $[\mathbf{4}-4NO_3]^{4+}$. The fragmentation reactions can be nicely followed by varying the irradiation time between 0.2–0.7 s (Figure 8). It is important to first note that no fragment is observed which only contains a Pt corner and one of the cytosine or uracil ligands. Such a fragment bearing Pd instead of Pt is, however, clearly observed at m/z: 372 after longer irradiation times. This finding indicates that the coordination to the Pt corner is more easily cleaved than that to the Pd corners, although the binding energies of the ligands to Pt^{II} are higher than to Pd^{II}. Two mechanisms can resolve this seeming contradiction: The coordination to Pd involves deprotonated N atoms for both ligands. Cleavage of a Pd–N bond would result in charge separation, which is energetically unfavorable. Instead, the cytosine N3 atom can dissociate from the Pt

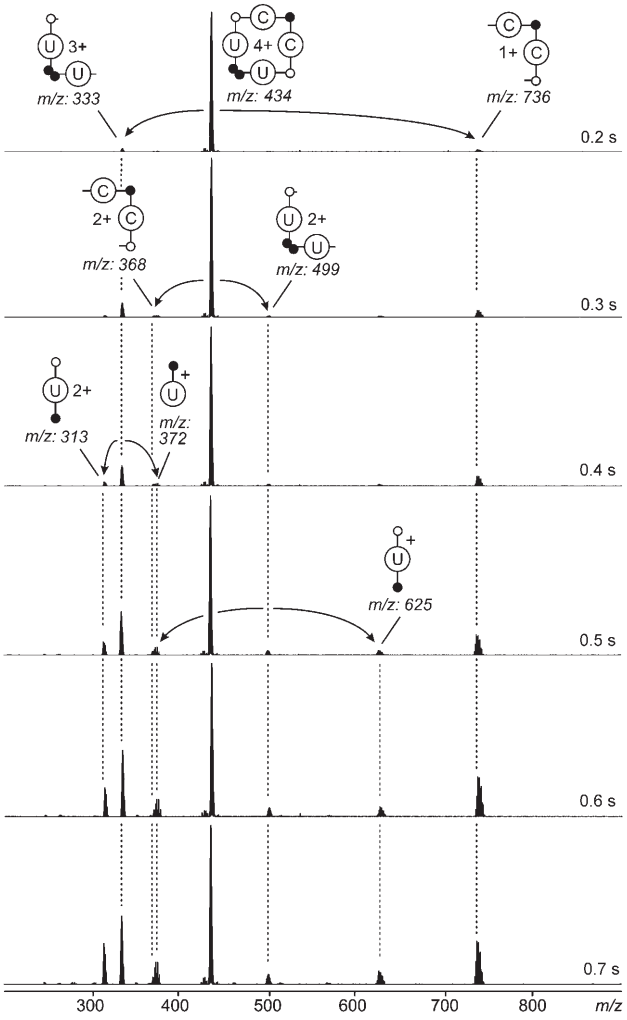

Figure 8. IR multiphoton dissociation (IRMPD) experiment conducted by irradiating mass-selected quadruply charged parent ions with a CO_2 laser (10.5 μM; 25 W). Due to the multiply charged nature of the parent, both fragments carry charges and are thus visible in the mass spectra. From top to bottom: Increasing irradiation times as given on the right-hand side. As the fragments are irradiated too, consecutive fragmentations can be observed as indicated.

corner without such a charge separation. Thus, simple cleavage of the Pt–N3C bond is one process. The second mechanism involves a 1,2-elimination reaction in which the nitrogen atom is protonated by one of the ethylene diamine protons. This reaction can only occur at the Pt corner, because the 2,2′-bpy ligands at the Pd centers do not bear any acidic protons.

If the fragmentation reaction in the MS/MS experiment is followed with increasing irradiation times, one initially (after 0.2 s) finds two fragments appearing at *m*/*z*: 333 (triply charged) and *m*/*z*: 736 (singly charged). After 0.3 s of irradiation with the CO_2 laser, two very similar product ions at *m*/*z*: 368 and 499 become visible; these are both doubly charged and differ from those at *m*/*z*: 333 and 736 merely by their charge states. Both can easily be rationalized by cleavages of Pt–N bonds within the metallacalixarene scaffold according to the two mechanisms discussed above. Changes of the charge state just require a proton transfer between both fragments. The triply charged fragment at *m*/*z*: 333 and the doubly charged fragment at *m*/*z*: 499 both contain the intact double Pd bridge between both uracil ligands. According to the crystal structure of **4**, the double bridge consists of two Pd ions coordinated strongly to one deprotonated uracil N atom and to the carbonyl group of the second uracil. The coordinative bonds to the carbonyl groups can be cleaved without the need for charge separation, while cleavage of the Pd–N bonds must involve charge separation due to the bpy ligand at the Pd centers. In line with these considerations, the triply charged fragment at *m*/*z*: 333 undergoes subsequent fragmentation along these O–Pd coordinative bonds and forms a doubly charged fragment at *m*/*z*: 313 and a singly charged fragment at *m*/*z*: 372 (Scheme 3). Analogous fragments are formed from the doubly charged ions at *m*/*z*: 499. The product ion at *m*/*z*: 372 appears again, concomitantly, with a singly charged fragment at *m*/*z*: 625.

This analysis of the MS/MS spectra provides information on the preferred cleavage sites and thus gives insight into the intrinsic reactivity of the isolated species,[29] which cannot easily be observed in solution due to the environment. The analysis is also fully consistent with the structure assignment made for **4**.

Isolated species with different connectivity: **Pt_2Pd_4 complex 7 with the sequence uracil, cytosine, uracil, cytosine**: Another product isolated from the **1**/[Pd^{II}(2,2′-bpy)] system and characterized by X-ray crystal structure analysis was [{Pt(en)}$_2$(*N1*-U-*N3*,*O4*)$_2$(*N3*-CH-*N1*,*O2*)$_2$Pd(2,2′-bpy)}$_4$]-(NO_3)$_6$ (**7**). The cation of **7** is depicted in Figure 9 and salient structural data are listed in Table 4.

The cation is composed of a tetranuclear, cyclic Pt_2Pd_2 core unit, in which the sequence of nucleobases is [(*N3*-U-*N1*)Pt(*N3*-CH-*N1*)Pd(*N3*-U-*N1*)Pt(*N3*-CH-*N1*)Pd] and is therefore different from the cases discussed so far (**2a**, **4**). The uracilate and cytosine nucleobases adopt a 1,3-alternate conformation as far as their substituents at the exocyclic positions are concerned, for example, the O2 atom of U and the O2 atom of CH. Two more [Pd^{II}(2,2′-bpy)] units, bonded pairwise through the O2 atom of the cytosine monoanion and the O4 of the uracil dianion, are added on top of the two other [Pd^{II}(2,2′-bpy)] entities, thereby forming *head–head* arrangements and short Pd···Pd contacts of 2.844(1) (Pd1···Pd2) and 2.815(1) Å (Pd1′···Pd2′). The geometry of the Pt_2Pd_2 core unit closely resembles that of [{Pt(en)(UH)}$_4$]$^{4+}$[1,2] as far as the intermetallic distances and overall arrangement of the pyrimidine bases (1,3-alternate) are concerned. As with the former, the four central metal ions (Pt1, Pt1′, Pd1, Pd1′) in **7** are in a butterfly arrangement, with deviations of 0.2525(3) (Pt1), 0.2580(3) (Pt1′), −0.2550(3) (Pd1), and −0.2555(3) Å (Pd1′) from the mean plane. The sides of the square range from 5.743(2)–5.917(2) Å. The diagonal intermetallic distances are 7.873(3) Å for Pt···Pt and 8.531(3) Å for Pd···Pd.

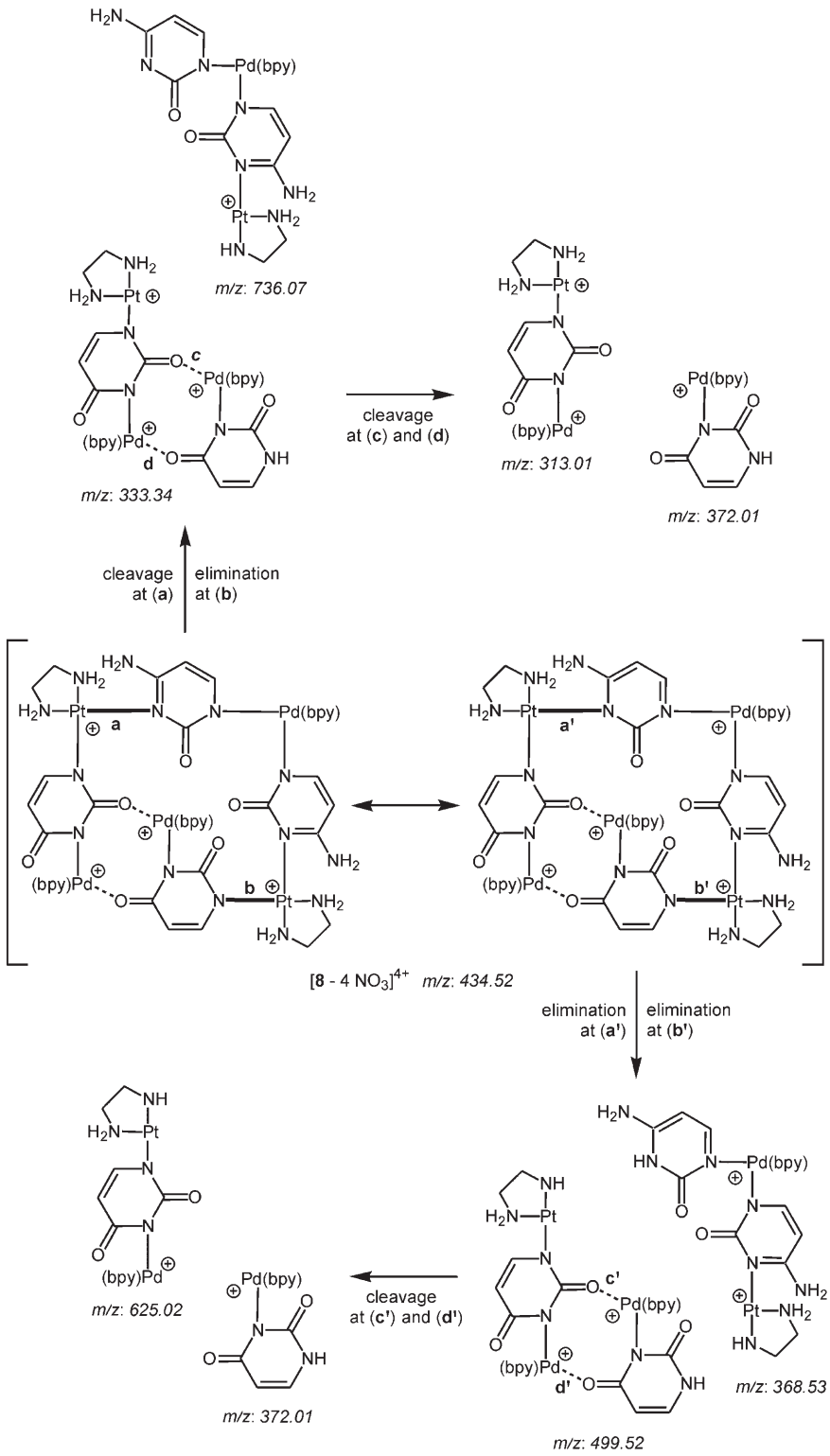

Scheme 3. Fragmentation pattern of complex **4** with mass-selected $[\mathbf{4}-4\,NO_3]^{4+}$, as observed in the IRMPD experiments.

Instability of 7: Compound **7** was isolated from a solution of **1** and $[Pd(2,2'\text{-bpy})(H_2O)_2]^{2+}$ upon complete evaporation of the solvent. When **7** is redissolved in D_2O, rapid changes take place in the ^1H NMR spectrum. A series of low-intensity nucleobase doublets ($\delta = 5.6$–6.5 ppm) appears rapidly, before signals due to compound **4** begin to dominate within one day. If NaCl is added to a freshly prepared solution of **7** in D_2O, there is a rapid precipitation of $[PdCl_2(2,2'\text{-bpy})]$ and formation of a new set of resonances assigned to an unknown species "**X**" (Figure 10). We assume that loss of the O-bonded $[Pd^{II}(2,2'\text{-bpy})]$ entities is the first step in this process and that the resonances marked with "**X**" in Figure 10 in fact correspond to the metallacalix[4]arene with the sequence uracil, cytosine, uracil, cytosine (compound **6**). The loss of the bpy resonances of **7** at $\delta = 7.3$ ppm, believed to be characteristic of stacked 2,2′-bpy entities, during the conversion of **7** into "**X**" is consistent with this assumption. Subsequent steps are unclear at present, particularly because compound **4**, with its different nucleobase connectivities, eventually forms (Figure 10, spectrum c). This is only possible if fragmentation of "**X**" and a rearrangement process take place.

Cyclic Pt_4Pd_4 complex 9a: **A metallacalix[8]arene**: $[\{Pt(en)(N1\text{-U-}N3)(N3\text{-CH-}N1)\}_4\{Pd(2,2'\text{-bpy})\}_4](NO_3)_3(ClO_4)\cdot 56.1\,H_2O$ (**9a**) is a cyclic, octanuclear complex comprising four $[Pt^{II}(en)]$ and four $[Pd^{II}(2,2'\text{-bpy})]$ entities, as well as four uracil dianions (U) and four cytosine monoanions (CH). Unlike related metallacalix[*n*]arenes with $n = 3$,[6] 4,[1,2,4] and 6,[7] compound **9a** with $n = 8$ no longer has the shape of a ring but rather adopts a strongly folded structure (Figure 11).

Compound **9a** crystallizes in space group $P4_2/n$ and has two crystallographically independent cations. The asymmetric unit features one entire octanuclear cation (complex I) as well as a quarter of a second cation. The latter complex

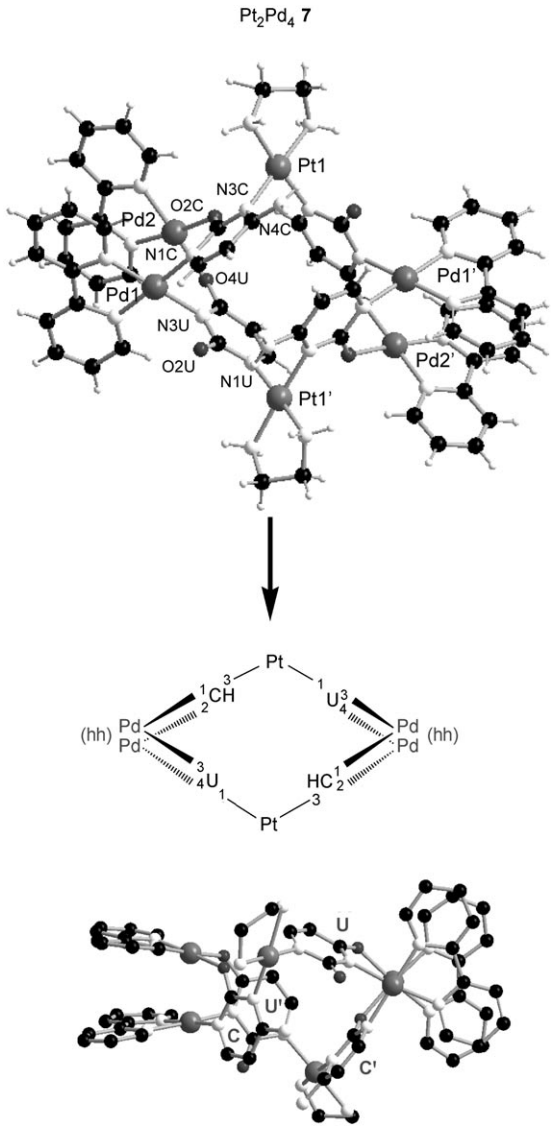

Figure 9. Views of Pt_2Pd_4 cation $[\{Pt(en)\}_2(N1\text{-}U\text{-}N3,O4)_2\{Pd(N3\text{-}CH\text{-}N1,O2)(2,2'\text{-bpy})\}_4]^{6+}$ (**7**) and a schematic representation of the connectivities.

Table 4. Selected interatomic distances [Å] and angles [°] in **7**.

Pt1–N1 (U)	2.017(6)	N11-Pt1-N12	83.0(3)
Pt1–N3 (C)	2.055(7)	N1 (U)-Pt1-N3 (C)	89.2(3)
Pt1–N11	2.022(7)	N11-Pt1-N1 (U)	94.4(3)
Pt1–N12	2.039(6)	N12-Pt1-N3 (C)	93.5(3)
Pd1–N3 (U)	2.025(7)	N11′-Pd1-N12′	80.7(3)
Pd1–N1 (C)	2.024(7)	N3 (U)-Pd1-N1 (C)	85.9(3)
Pd1–N11′	2.022(7)	N11′-Pd1-N3 (U)	96.9(3)
Pd1–N12′	1.988(7)	N12′-Pd1-N1 (C)	96.5(3)
Pd2–O4 (U)	2.021(6)	N11′-Pd2-N12′	81.4(3)
Pd2–O2 (C)	2.026(7)	O4 (U)-Pd2-O2 (C)	92.5(3)
Pd2–N11′	1.984(7)	N11′-Pd2-O4 (U)	93.2(3)
Pd2–N12′	1.982(7)	N12′-Pd2-O2 (C)	93.1(3)
Pd1···Pd2	2.844(1)		

fragment is arranged around a crystallographic fourfold inversion axis which generates the complete complex (complex II). Complex I likewise possesses a (in this case, noncrystallographic) fourfold inversion axis, which runs through the center of the cation. Thus, the geometries of complexes I and II are nearly identical. The cytosine and uracil nucleobases are clearly distinguishable by means of the lengths of the C4–N4 bonds as compared to the carbonyl bonds, as well as on the basis of the thermal displacement factors of the N and O atoms.

Within each complex, uracilato and cytosinato ligands alternate, thereby leading to alternation of the N1 and N3 sites of the pyrimidine bases and hence to (uracil, cytosine, uracil, cytosine)$_2$ connectivities. The four Pt atoms form a distorted tetrahedron with Pt···Pt distances of 9.579(1)–10.972(2) Å, as do the 4 Pd atoms, albeit with shorter distances (7.789(2)–8.889(2) Å). The four metals "at the bottom" (Pt3, Pt4, Pd3, Pd4) and likewise the four metals "at the top" (Pt1, Pt2, Pd1, Pd2) form a rhomboid, each with slight deviations of approximately ± 0.2 Å of the metal atoms from planarity, thereby resulting in a butterfly arrangement. The sides of each rhomboid are defined by two shorter and two longer Pt···Pd distances, distances that range from 5.789(1)–5.854(1) Å and 7.766(1)–8.210(1) Å, respectively. The diagonal intermetallic distances amount to 10.605(2)–10.972(2) Å (Pt···Pt) and 8.671(2)–8.889(2) Å (Pd···Pd). If the 2,2′-bpy and en ligands are also taken into account and the van der Waals radii are included, the largest expansion of the cylinder-shaped Pt_4Pd_4 cation is approximately 16.1 (diameter) × 15.8 Å (height). Views along the fourfold inversion axis of cation I and from the side are given in Figure 12. Uracilato and cytosinato are mutually *head–tail* oriented (with respect to their O2 groups), with the following angles between the metal coordination planes and the nucleobases: CH/Pt 75.2(2)–83.0(2)°, U/Pt 69.5(2)–81.1(2)°, CH/Pd 58.2(2)–63.7(2)°, U/Pd 71.4(2)–82.1(2)°. All four CH bases have their C5,C6 faces directed into the interior of the cation and pointing up, down, up, down. This arrangement might be a direct consequence of the bulky bipyridine ligands, as the relatively short contacts of ≈3.4 Å between the C5 atoms of the cytosine bases and the C6 atoms of the neighboring bpy ligands hinder rotation of the bases out of the inner cavity. A rotation of the cytosine bases in the other direction, and thus even further into the cavity, would shorten the hydrogen bond between the cytosine amino groups and the O2 positions of neighboring, Pt-linked uracil bases (≈3.1 Å). However, this is hindered by a possible steric clash between the O2 atoms of the cytosine bases and the O4 atoms of the neighboring, Pd-linked uracil bases (distance ≈3.5 Å). The top and bottom of each cation is closed by a tight hydrogen-bonding network involving the O2 positions of both uracilates, the N4–H_2 groups of both cytosinates, and two water molecules per opening (Figure 13). In detail, each O2 atom is connected through one water molecule (H_2O···O2, mean distance 2.73(2) Å) to the N4–H_2 group on the opposite side of the opening (H_2O···N4–H_2, mean distance 2.92(2) Å), while the second

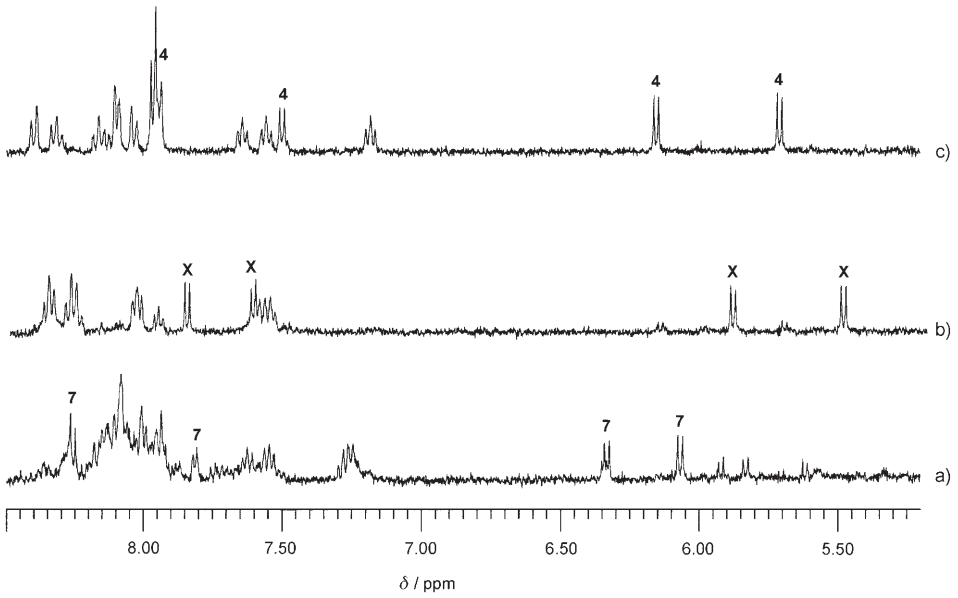

Figure 10. Low-field sections of the ^{1}H NMR spectra of compound **7** when it is redissolved in D_2O with NaCl added, as it is converted into compound **4**: a) Immediately after sample preparation (pD = 7.23), b) after 2 h, and c) after 1 day.

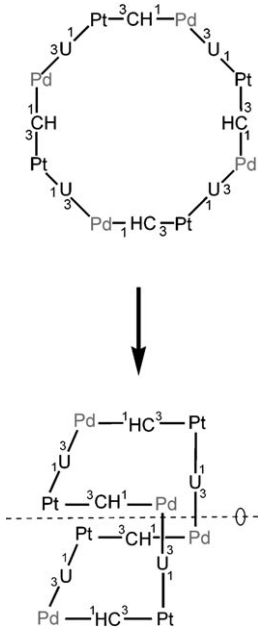

Figure 11. Schematic representations of cyclic Pt_4Pd_4 compound **9a**.

acceptor site of each O2 is involved in a hydrogen bond to the second donor site of the neighboring N4–H_2 group (O2···N4–H_2, mean distance 3.08(2) Å). The two water molecules, bound tightly in each opening in the above described way, additionally form a hydrogen bond with each other (H_2O···H_2O, mean distance 2.80(2) Å). Selected interatomic distances and angles are listed in Table 5.

Inspection of the crystal packing reveals that the main difference between complexes I and II is due to the intermolecular interactions they form with neighboring complex cations (see the Supporting Information). Both sorts of cations are arranged with their fourfold inversion axes parallel to the *c* axis, thereby forming infinite tubes along the *c* direction, intersected only by anions and water molecules. Perpendicular to the *c* axis, these tubes are connected by stacking interactions between the 2,2′-bpy ligands of neighboring cations with distances of 3.28(4) and 3.43(4) Å and angles between the 2,2′-bpy planes of 1.9(3) and 6.7(3)°. While complex II, due to its fourfold crystallographic symmetry, engages all four bpy ligands in this kind of interaction, complex I only forms three such contacts while the two nitrogen atoms of the fourth bpy ligand (N12 and N12′ at Pd2) are in close proximity to the en ligand of Pt2 (N12···C12e 3.63(1) Å, N12′···C12e 3.78(1) Å). Overall, the packing results in a pattern in which tubes consisting of complex II are rotated by roughly 20° parallel to the *c* axis, relative to tubes formed by complex I. Anions and water molecules form a complicated, though rather flexible, network by filling the relatively large space between the complex cations, especially the holes between cations arranged in tubes along the *c* axis. The positions of anions and water molecules are rather poorly defined (see the Experimental Section).

^{1}H NMR spectrum of 9a: The ^{1}H NMR spectrum of **9a** in D_2O is simple, with only single doublets for H5 ($\delta = 5.10$ and 5.61 ppm) and H6 ($\delta = 6.54$ and 7.68 ppm) resonances observed for the two nucleobases and altogether eight resonances for the bpy ligands derived from the two nonequivalent halves of each 2,2′-bpy (see the Supporting Information). The relative intensities of the protons of the nucleobases and the 2,2′-bpy ligands are in agreement with expectations. One of the bpy resonances, a triplet at $\delta = 6.95$ ppm, stands out amongst all of the bpy signals because of its high upfield shift. Inspection of the solid-state structure of **9a** suggests that this signal is due to the H5 proton of the pyridine ring *trans* to the uracil N3 donor atom, which gives rise to this upfield shift because of its disposition underneath a uracil ring. Spectral changes are observed within several hours at room temperature. Within two days, the resonances of **9a** have disappeared completely and two sets of uracil and cytosine resonances, each with relative intensities of 2:1, have formed instead. These resonances can be readily assigned to **4** and **1**, respectively (see the Supporting Informa-

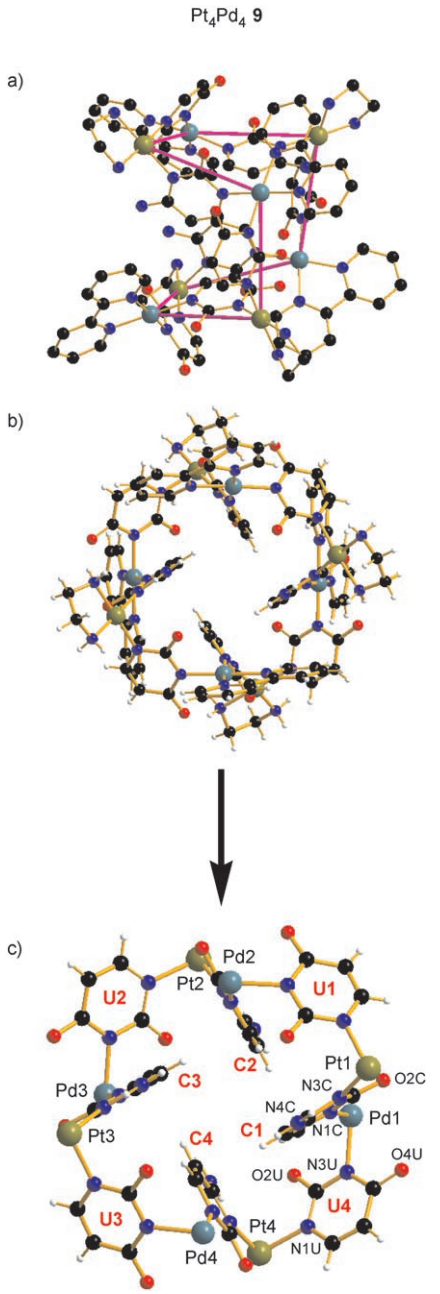

Figure 12. Different views of octanuclear Pt_4Pd_4 cation **9a**: a) Side view, b) view along the fourfold inversion axis, and c) view along the inversion axis with the en and 2,2′-bpy ligands omitted for clarity.

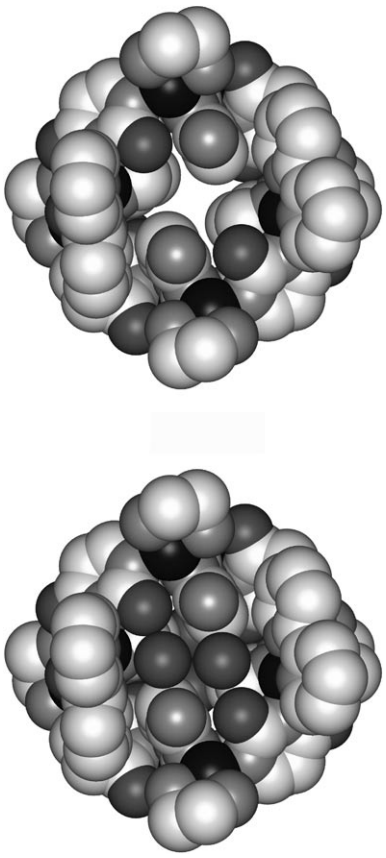

Figure 13. Space-filling representation of cation **9a** viewed along the fourfold inversion axis: without water molecules (top) and with two water molecules included in the inner cavity from each side (bottom).

Table 5.
Selected interatomic distances [Å] and angles [°] in **9a**.[a]

Pt–N1 (U)	2.007(7)–2.040(8)	N (en)-Pt-N (en)	83.1(4)–84.1(3)
Pt–N3 (C)	2.024(7)–2.050(7)	N1 (U)-Pt-N3 (C)	88.5(3)–90.2(3)
Pt–N (en)	1.994(7)–2.041(8)	N (en)-Pt-N1 (U)	92.4(3)–93.5(3)
Pd–N3 (U)	2.019(7)–2.025(7)	N (en)-Pt-N3 (C)	93.5(3)–94.5(3)
Pd–N1 (C)	2.021(7)–2.038(8)	N (bpy)-Pd-N (bpy)	80.0(3)–80.7(3)
Pd–N (bpy)	1.996(8)–2.041(8)	N3 (U)-Pd-N1 (C)	84.7(3)–86.4(3)
		N (bpy)-Pd-N3 (U)	95.6(3)–97.0(3)
		N (bpy)-Pd-N1 (C)	97.3(3)–98.1(3)

[a] For the two crystallographically independent cations, maximum and minimum values are given.

tion) and indicate a clean conversion of **9a** into **4** and **1** according to $3\times$**9a**$\rightarrow 4\times$**4**$+4\times$**1**.

Different connectivities through different reaction routes: The different connectivities of the nucleobases in **2a** and **4** on one hand and in **7** and **9a** (and probably also in "**X**") on the other strongly suggest that different pathways lead to the formation of the individual compounds. In Figure 14, possible reaction schemes for the formation of **4**, **7**, and **9a** are outlined, and a more detailed scheme for possible pathways leading to the formation of **9a** is provided in Figure 15. Arrows given in these figures indicate feasible pathways but do *not* indicate one-way reactions. In fact, the formation of **4** from **7** and the concomitant alternations in ligand connectivities strongly indicate equilibria; hence, there is also the possibility to reverse pathways. Only boxed-in species have been characterized by X-ray crystal structure analysis. From Figure 14, it becomes evident that the relative ratio of Pt starting compound **1** versus [Pd^{II}(2,2′-bpy)] ("Pd") influences the composition of the initial compound (**2a**–**2c** versus **5a**, **5b**) and that calix[4]arenes **3** and **6** can be obtained through two routes. Moreover, the way that open products condense ("self-sorting" or heterodimerization) has an influ-

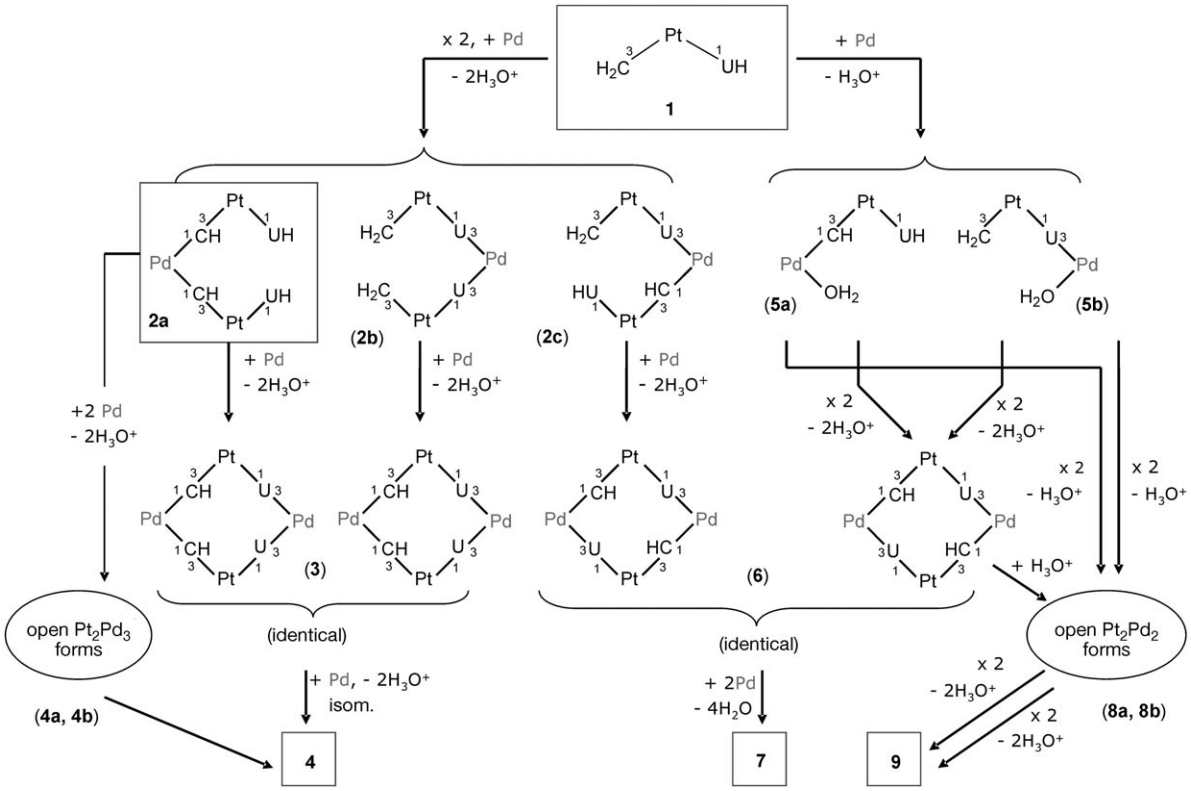

Figure 14. Possible pathways leading from $[Pt(en)(UH\text{-}N1)(CH_2\text{-}N3)]^+$ (**1**) to multinuclear species. "Pd" denotes $[Pd(2,2'\text{-bpy})(H_2O)_2]^{2+}$.

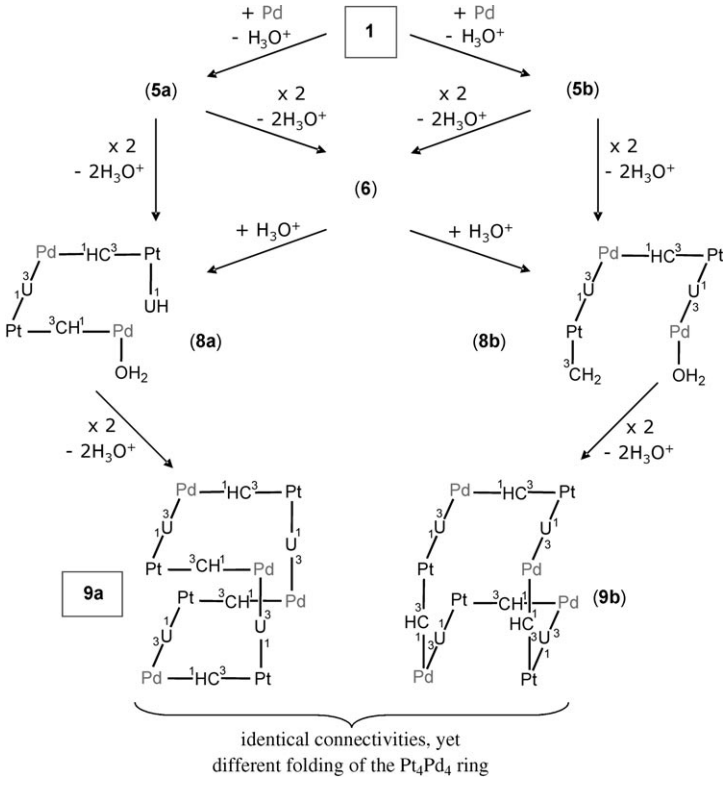

Figure 15. Possible pathways leading to the metallacalix[8]arene **9a**.

ence on the connectivity of the resulting macrocyclic ring. For example, heterocondensation of **5a** and **5b** can likewise lead to **3** (not shown in Figure 14). On the other hand, formation of **9a** conceivably takes place through self-sorting of **8a** (Figure 15). Self-sorting of **8b** leads to species **9b** with identical connectivities to those seen in **9a**, yet with a different folding topology of the Pt_4Pd_4 ring. From model building it is evident that there are numerous feasible foldamers other than **9a** and **9b**, but it appears unlikely that rapid interconversion between the various forms is possible. It is also obvious that heterocondensation between **8a** and **8b** leads to foldamers with some of the connectivities being different from those in **9a** and **9b**.

Reaction products of 1 with $[Pd^{II}(en)]$: As compared to the results from the **1**/$[Pd^{II}(2,2'\text{-bpy})]$ system discussed so far, the number of fully characterizable species obtained from **1** and $[Pd^{II}(en)]$ was much smaller. The first compound isolated proved to be a cyclic tetramer consisting of two $[Pt^{II}(en)]$, two $[Pd^{II}(en)]$, two uracilate dianions, and two cytosinate monoanions, $[\{Pt(en)\}_2U_2(CH)_2\{Pd(en)\}_2](NO_3)_2$ (**Y**), according to a mass spectrometry study (see below). The question of connectivity in **Y**, which may be of structure **3′** (an analogue of **3**, Figure 14) or of structure **6′** (an analogue of **6**), is not readily answered on the basis of the ^1H NMR spectra. The compound is perfectly stable in neutral aqueous solution, even upon heating to 70 °C (with gradual isotopic exchange of the uracil H5 proton) and in

the presence of a large excess of NaCl (>50 equivalents). Only in DCl does decomposition into **1** and $[PdCl_2(en)]$ take place, and the formation of **1** is likewise observed at pD 13.

The assignment of the ^1H NMR resonances of **Y** with its two sets of uracil and cytosine resonances was achieved by a combination of 2D $^1H,^1H$-NOESY and 2D $^1H,^{13}C$-COSY experiments (Table 1 and the Supporting Information), with the help of direct and long-range $^1H,^{13}C$ coupling. Attempts to apply NOESY techniques in $[D_6]$DMSO, to get an insight into the neighborhood of the amino protons of the cytosine ligands and hence the connectivity pattern, failed because of complex decomposition in this solvent.

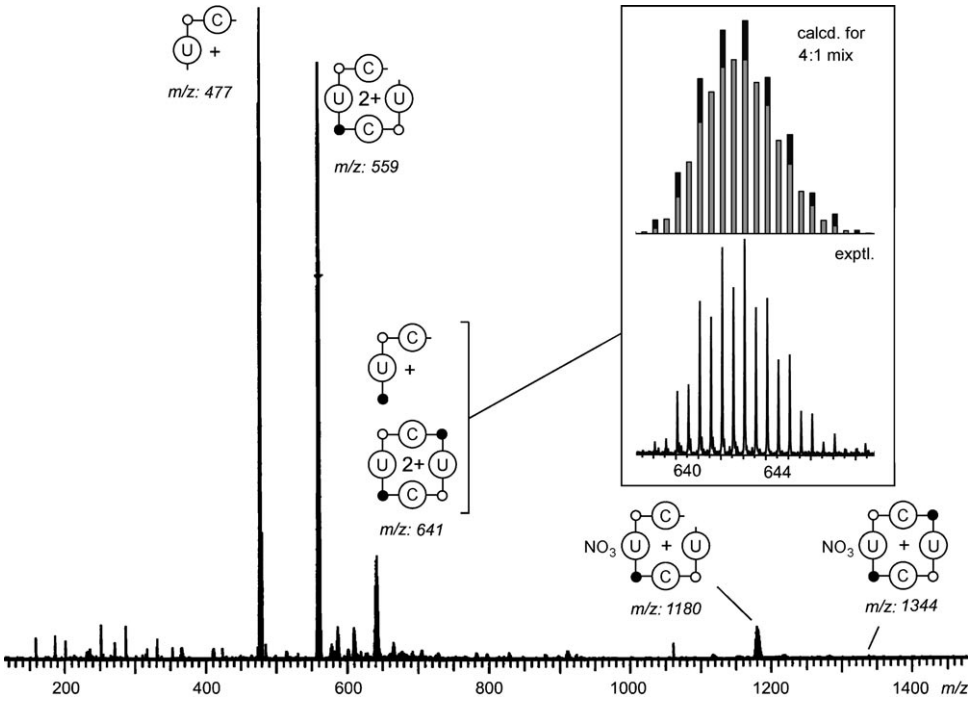

Figure 16. ESI-FTICR mass spectrum obtained from a 150 μM solution of **Y** in methanol/water (approximately 1:1). Assignment of the observed signals to structures is indicated by the graphics (Pt: open circles, Pd: filled circles). The inset shows the isotope pattern found for the ions at *m*/*z*: 641 and compares it to a 4:1 superposition of the patterns calculated for $[\mathbf{Y}-2NO_3]^{2+}$ and its singly charged half, as indicated above the corresponding peaks.

Irrespective of the question of nucleobase connectivities in compound **Y**, we were also interested in the possible conformation of this metallacycle. Consistent with our previous experimental findings[4] and with the model building for **Y**, the cone conformer (O2 groups of all four nucleobases pointing in the same direction) can be expected to provide access to anions from the side opposite to the O2 oxygen atoms and hence to behave as a host for anionic guests. In order to probe such a possibility, we added increasing amounts of 3-trimethylsilylpropanesulfonate (TSP) to an aqueous solution of **Y**. There was no effect whatsoever on the chemical shifts of any of the resonances, a result strongly suggesting that compound **Y** does not adopt a cone structure but rather is in a 1,3-alternate conformation.

MS study of Pt_2Pd_2 (Y): As **Y** could be isolated on a preparative scale and analyzed as $[\{Pt(en)\}_2U_2(CH)_2\{Pd(en)\}_2](NO_3)_2$, it was studied in more detail. ESI-FTICR mass spectrometry confirmed the composition of **Y**. In the mass spectrum obtained upon electrospraying an approximately 150 μM solution of **Y** in methanol/water (1:1 v/v), quite intense signals were observed for the doubly charged $[\mathbf{Y}-2NO_3]^{2+}$ at *m*/*z*: 641.06 (Figure 16). Consequently, the assembly is easily ionized by stripping away the two counterions. The isotope pattern of this ion is superimposed by a singly charged fragment which corresponds to half the macrocycle and thus appears at the same *m*/*z* value. The relative intensities of the parent dication and its singly charged fragment can be estimated to amount to approximately 4:1 (see the inset in Figure 16). Two other signals appear with high intensities: a dication at *m*/*z*: 559.08 and a monocation at *m*/*z*: 477.10. They can both be rationalized by invoking the loss of an $[Pd(NHCH_2CH_2NH)]$ corner from $[\mathbf{Y}-2NO_3]^{2+}$ or its fragment, respectively, as depicted in Scheme 4. All fragments can be formed through the same elimination mechanism which involves deprotonation of the NH_2 groups of the en ligands at the Pd center. In contrast to the 1,2-elimination processes discussed above for **4**, it is now the Pd corner at which this process occurs, as expected from the different binding energies of the nitrogen ligands to Pd^{II} and Pt^{II}. Two different mechanistic alternatives seem reasonable to rationalize the ease of this process, which indeed even occurs under the soft conditions of electrospray ionization: A simple 1,2-elimination or a reaction proceeding through a six-membered transition structure (see the inset in Scheme 4). The products are keto–enol tautomers, which are not easily distinguished by mass spectrometry experiments. The abstraction of one of the en NH_2 protons in each of these steps again avoids the energy-demanding charge separation processes that would be required if a simple N–metal bond cleavage were to occur in the fragmentation reaction. Singly charged $[\mathbf{Y}-NO_3]^+$ ions and a similar series of fragments also appear in the mass spectrum, although with much lower intensities.

A tandem MS experiment with mass-selected $[\mathbf{Y}-2NO_3]^{2+}$ provides information about the fragmentation pattern. In this IRMPD experiment, no singly charged fragments were observed at *m*/*z*: >641. This indicates that the

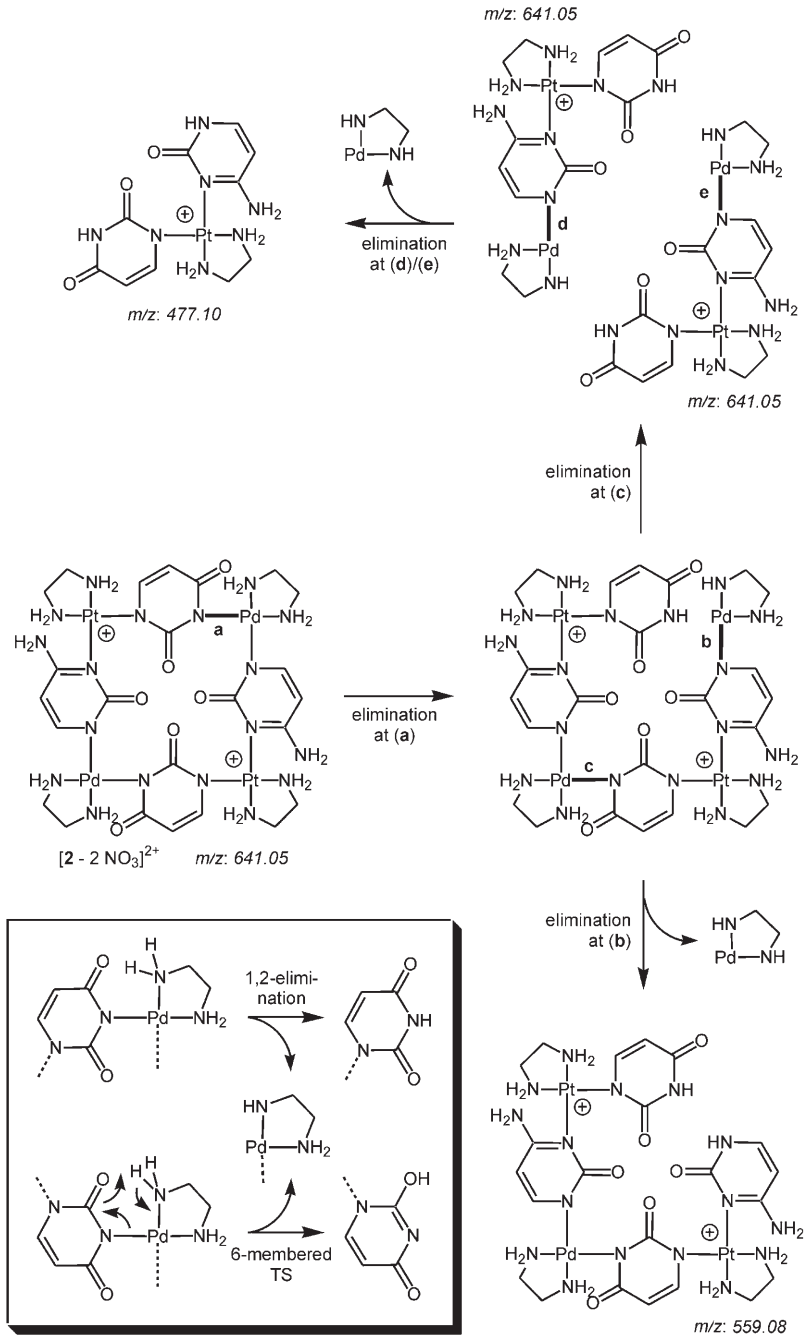

Scheme 4. Rationalization of fragments observed in the ESI mass spectrum of **Y**. Two different mechanisms may account for the observed dissociation reactions (inset). The products differ only by a keto–enol tautomerism and cannot be distinguished easily by mass spectrometry.

major fragmentation pathway is dissociation of the $[\mathbf{Y}-2NO_3]^{2+}$ dication into two identical, singly charged halves. Any other, nonsymmetrical fragmentation reaction with two singly charged fragments as the products would necessarily generate one fragment above and one below *m*/*z*: 641. In addition, small signals for the dicationic fragment at *m*/*z*: 559 and intense signals at *m*/*z*: 477 were observed, in line with the mass spectrum. However, the ion at *m*/*z*: 559 represents a major species in the ESI mass spectrum, while it appears only with low intensity in the MS/MS spectrum. Thus, some doubts remain that it is exclusively formed as a fragment upon ionization.

The fragmentation pattern given in Scheme 4 is based on the assumption that compound **Y** possesses the uracil, cytosine, uracil, cytosine connectivity. We admit that we have at present no way to unambiguously rule out the second possibility discussed above.

Pt_2Pd_6 complex 11′ with uracil, cytosine, uracil, cytosine connectivity: The only compound from the system **1**/[Pd^{II}(en)] that was isolated as a single crystal and subsequently studied by X-ray crystallography was the octanuclear complex [{Pt(en)(U-*N1*,*N3*,*O2*,*O4*)(C-*N1*,*N3*,*N4*,*O2*)}$_2$[Pd(en)}$_6$]-$(NO_3)_5(ClO_4)_3$•21.2 H_2O (**11′**). It was not an analogue of any of the compounds characterized in the system **1**/[Pd^{II}(2,2′-bpy)] and was obtained from a solution containing a large excess of [Pd^{II}(en)] over **1**. Its occurrence in solution (spectrum d in Figure 3) was established only after obtaining a ^{1}H NMR spectrum of isolated **11′**.

A view of the cation of **11′** is given in Figure 17 and selected structural details are listed in Table 6. Complex **11′** crystallizes in the tetragonal space group $I4_1/a$ with a quarter of an octanuclear cation forming the asymmetric unit. The octanuclear species is generated through the fourfold inversion axis in the center of the molecule. Consequently, the uracil and cytosine rings are indistinguishable. The exocyclic group at the C2 position was treated as a carboxyl group, although 50% of the positions are occupied by amino groups of the cytosine moieties. Additionally, Pt and Pd atoms cross-linking the N1 and N3 sites occupy identical positions and were assigned 50% occupancy, respectively. The four nucleobases of each cation enclose a cavity. This cavity is cut in half by the $Pt1_2Pd1_2$ plane. Opposite nucleobases are positioned

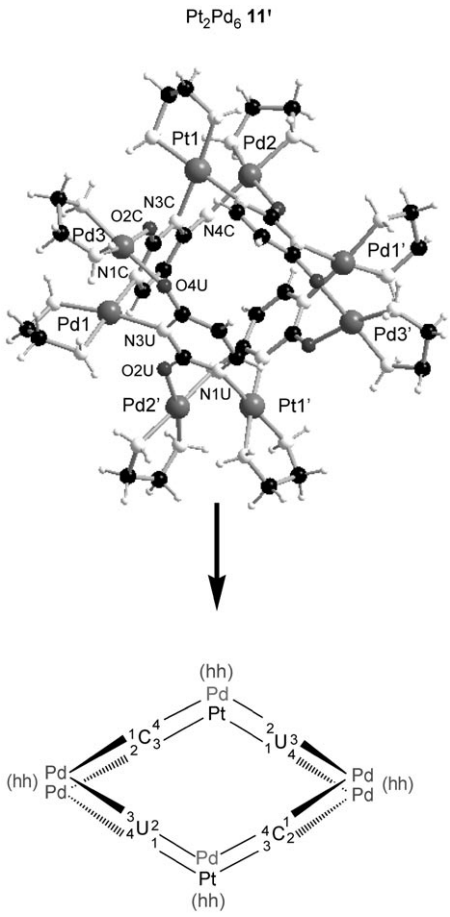

Figure 17. Views of octanuclear Pt_2Pd_6 cation **11′** and a schematic representation of the cation composition.

Table 6. Selected interatomic distances [Å] and angles [°] in **11′**.

Pt1−N1	2.032(7)	N11-Pt1-N12	83.5(4)
Pt1−N3#1[a]	2.033(7)	N1-Pt1-N3#1[a]	87.6(3)
Pt1−N11	2.054(7)	N11-Pt1-N1	95.3(3)
Pt1−N12	2.060(7)	N12-Pt1-N3#1[a]	93.6(3)
Pd1−N1	2.032(8)	N11-Pd1-N12′	83.3(4)
Pd1−N3#1[a]	2.036(8)	N1-Pd1-N3#1[a]	87.5(3)
Pd1−N11′	2.058(8)	N11′-Pd1-N1	95.2(4)
Pd1−N12′	2.065(8)	N12′-Pd1-N3#1[a]	93.4(4)
Pd3−N21	1.989(8)	N21-Pd3-N22	83.4(4)
Pd3−N22	2.024(8)	O2-Pd3-O4#1[a]	95.5(3)
Pd3−O2	2.039(6)	N21-Pd3-O2	90.1(3)
Pd3−O4#1[a]	2.009(7)	N22-Pd3-O4#1[a]	89.9(3)
Pt1···Pd2	3.04(1)		
Pd1···Pd3	2.96(3)		

[a] #1: $-y+{}^{7}/_{4}$, $x-{}^{1}/_{4}$, $-z+{}^{3}/_{4}$.

above and below this plane, respectively, and are tilted towards each other, thus minimizing the C5···C5 distances and forming angles of 65.7(2)° to the $Pt1_2Pd1_2$ plane. Neighboring nucleobases enclose angles of 80.3(2)°. The maximum diameter of the inner core of the complex can be estimated by the C2···C2 distance of opposite nucleobase rings, which amounts to 5.68(2) Å. The size of the two openings of this core is defined by the C5···C5 distances of opposite rings (3.54(2) Å). The distance of the C5 atoms to the $Pt1_2Pd1_2$ plane is 2.88(1) Å; thus, the height of the inner core can be estimated to be 5.76 Å. Planes defined by the coordination spheres of the heavy metals, that is, $Pt1N_4$ or $Pd1N_4$ and $Pd2N_4$, form angles of 38.6(3)° with each other. No guest molecules can be accommodated inside the cavity. Anions and water molecules fill the space between complexes and are partially bound to the outer sphere of the cation through the amino groups of the en ligands. Possibly due to the relatively wide space between individual cations, the network between the anions and water molecules permits a high degree of dynamics, which explains the poorly defined positions of the counterions and solvent molecules inside the crystal lattice. Details are given in the Experimental Section.

The relationship of 11′ with M_8U_4: Formally, the structure of **11′** can be derived from the cyclic tetranuclear Pt_2Pd_2 compound **6′** (an analogue of **6**; compare with Figure 14), in which all four bases are cross-linked in an alternating 1,3 fashion to ring N atoms of the four nucleobases, upon addition of four more $[Pd^{II}(en)]$ residues to the eight available exocyclic sites. The extra $[Pd^{II}(en)]$ residues are attached pairwise to the uracil O4 and cytosine O2 sites, as well as to the uracil O2 and cytosine N4 sites. All four nucleobases are dianions, with uracil deprotonated at the N1 and N3 positions and cytosine deprotonated at the N1 site and at the exocyclic amino group of the N4 atom. Thus, in **11′** all four bases act as tetradentate ligands. The cation of **11′** has a very close structural similarity with related Pt_8U_4 and $Pt_4Pd_4U_4$ complexes previously reported by us.[5a] This similarity includes intermetallic distances within the cation. Superficially, the main difference between the U_4 and the U_2C_2 compounds is that the exocyclic O4 oxygen atoms of two uracil ligands in Pt_8U_4 are replaced by two isoelectronic N4−H groups (to give two cytosinate ligands) in **11′**. If the fact that two different nucleobases are present in **11′** is ignored and with consideration of the O2 groups only, even the 1,3-alternate arrangement of the four pyrimidine bases is identical. The four heavy metals cross-linking the endocyclic N1 and N3 sites of the four nucleobases in **11′** are not in a plane. Rather they adopt a flat butterfly structure, with two metals, for example, Pt1 and Pt1′, slightly above the best mean plane (0.11(1) Å) and the other two metals, Pd1 and Pd1′, slightly below this plane (−0.11(1) Å).

Pd_2Pd_4 complex 10′: When **11′** is dissolved in D_2O, there is rapid formation (within minutes) of new ^{1}H NMR spectroscopic resonances, due to partial loss of $[Pd^{II}(en)]$ from the cation. This is evident from the appearance of signals due to free $[Pd(en)(D_2O)_2]^{2+}$ ($\delta = 2.51$ ppm, pD 4.65) in the ^{1}H NMR spectrum. The simplicity of the resulting spectrum, which is consistent with the presence of only one type of uracil and one type of cytosine ligand (see the Supporting Information) and the intensity of the resonance due to uncoordinated $[Pd(en)(D_2O)_2]^{2+}$ reveal that two of the six $[Pd^{II}(en)]$ entities are lost. We assume that it is the two Pd^{II}

ions bonded pairwise to the O2 atom of cytosine and the O4 atom of uracil that are displaced, whereas the [Pd^{II}(en)] entities bonded to the deprotonated N4 position of cytosine as well as the O2 atom of uracil remain associated with the cycle under these conditions. We assign the species formed to "Pt_2Pd_4" (**10′**; Scheme 5). Resonances of **10′** are also present in mixtures of **1** and [Pd^{II}(en)] (see Figure 3). Compound **10′** is stable in D_2O under moderately basic conditions (pD 9.7), in the presence of a 50-fold excess of NaCl, and when heated to 70 °C for one day. In the latter case, there is accelerated exchange of the H5 protons by deuterium, with uracil exchanging faster. Only with DCl (pD < 1) is there decomposition to the starting compound **1**, again accompanied by isotopic exchange of the uracil H5 proton.

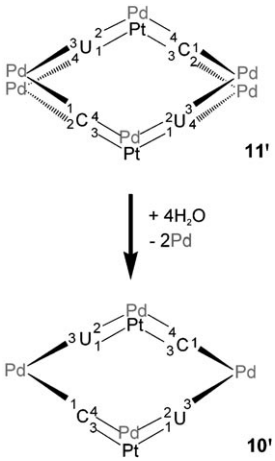

Scheme 5. Loss of [Pd^{II}(en)] from Pt_2Pd_6 (**11′**) to form **10′**.

When the excess of NaCl is further increased (100 equiv), **10′** starts to decompose into compound **Y** and the starting compound **1**.

Given the rapid loss of two [Pd^{II}(en)] moieties from **11′** in aqueous solution, it did not come as a surprise to see that similar ^{1}H NMR spectroscopic changes occur in the presence of good ligands, such as 9-methylguanine (9-MeGH) or adenosine monophosphate (AMP). Addition of two equivalents of 9-MeGH or one equivalent of AMP led to **10′** and a mixture of [Pd^{II}(en)] complexes with these nucleobases (not further identified), with **10′** being stable for days. Only when more 9-MeGH (4 equiv) was added was there partial decomposition of **10′**, which led eventually to **Y** and **1**.

Conclusion

In this study, a series of multinuclear, mixed-metal (Pt_x,Pd_y), mixed-nucleobase (uracil, cytosine) and, in part, mixed-amine (en; 2,2′-bpy) complexes have been characterized and their inter-relationships and ways of formation have been discussed. With one exception (compound **2a**), the adducts of **1** with either [Pd^{II}(2,2′-bpy)] or [Pd^{II}(en)] are cyclic compounds, collectively named metallacalix[*n*]arenes. Several examples with $n=4$ were characterized by X-ray crystallography, as was an unprecedented one with $n=8$. The availability of exocyclic functions of the nucleobases capable of chelating additional square-planar metal entities, namely O2 and O4 in uracil and O2 and N4 in cytosine, permits formation of metallacalix[4]arene compounds with altogether five (compound **4**), six (compound **7**), and eight (compound **11′**) metals bonded. Binding of the "extra" metal ions can occur exclusively through the exocyclic groups (**7**, **11′**) or in a mixed fashion (endocyclic N and exocyclic O atoms) as seen in **4**. The major structural differences between the compounds studied here are their different nucleobase connectivities, that is, UCUC in "**X**" (**6**), **7**, **9a**, and **11′**, yet UCCU in **2a** and **4**. The determining factors concerning connectivity are the binding patterns of the first Pd^{II} species to interact with the starting compound **1** (reaction at the uracil N3 or cytosine N1 atoms), the stoichiometry of the first species formed (Pt_2Pd or PtPd), and the dimerization patterns of these early products. Connectivities can be reversed (see, for example, conversion of **7** into **4**), a fact suggesting that complex fragmentation with Pd–N (nucleobase) bond breakage takes place and allows interconversion of species, as is characteristic of dynamic combinatorial chemistry.

In all of the structurally studied examples of metallacalix[4]arenes reported here (**4**, **7**, and **11′**), the four nucleobases adopt 1,3-alternate conformations in the solid state, irrespective of the nucleobase connectivity. As a consequence of this conformation, the interior of the metallacalix[4]arene does not have any space for inclusion of an anion or of solvent molecules, unlike a cone conformer, which provides a suitable hydrophobic cavity. The solution study with the Pt_2Pd_2 complex "**Y**" shows no evidence of ligand rotation to form a cone conformer either. It is possible that steric interference between the exocyclic amino group of the cytosine nucleobase and the H6 atom of the uracil nucleobase, which is to be expected both for UCUC and UCCU connectivities, prevents the cone conformation from being easily realized.

The chemistry carried out here does not answer all of the questions related to the so-called "platinum pyrimidine blues" derived from unsubstituted uracil. However, the trick of substituting slowly reacting *cis*-$Pt^{II}(NH_3)_2$ entities in part by faster reacting *cis*-$Pd^{II}a_2$ analogues and by preventing at the same time a sluggish Pt redox chemistry, which leads to mixed-valence compounds, has allowed us to understand some of the structural complexity, which most likely is shared by the "blues".

Experimental Section

Materials and methods: $[PtCl_2(en)]$,[30] $[PdCl_2(en)]$,[31] $[PdCl_2(2,2'\text{-bpy})]$,[31] and [Pt(en)(UH-*N1*)]Cl·H_2O[16] were prepared according to published procedures. Uracil and cytosine were of commercial origin (Fluka), as were 9-methylguanine (Chemogen), adenosine monophosphate (Sigma), and 2,2′-bipyridine (Aldrich).

[Pt(en)(UH-*N1*)(CH_2-*N3*)]NO_3·3.5H_2O (1a): [Pt(en)(UH-*N1*)]Cl·H_2O (302 mg, 0.720 mmol) and cytosine (80 mg, 0.72 mmol) were mixed in H_2O (80 mL) and kept at 40 °C for 4 days. After filtration of some ele-

mental Pt, $AgNO_3$ (120 mg, 0.98 equiv) was added. The mixture was stirred for 12 h at room temperature, filtered to remove AgCl, and concentrated by rotary evaporation to 1/10th of the original volume. $NaNO_3$ (61 mg, 0.72 mmol) was then added and the solution was kept at 4 °C. Within 7 days, colorless cubes formed, which were filtered off, washed with a small amount of ice water, and dried in air. Yield: 53 %; elemental analysis: calcd (%) for $C_{10}H_{16}N_8O_6Pt{\cdot}2H_2O$ (575.4): C 20.8, H 3.5, N 19.5; found: C 20.6, H 3.3, N 19.5. X-ray analysis showed the water content of freshly prepared **1a** to be higher (3.5 hydrate).

[Pt(en)(UH-*N1*)(CH$_2$-*N3*)]ClO$_4$·3H$_2$O (1b): The compound was obtained in an analogous way to that used for the synthesis of **1a** but with $AgClO_4$ applied. Compound **1b** was isolated in 50 % yield; elemental analysis: calcd (%) for $C_{10}H_{22}N_7O_{10}ClPt$ (630.86): C 19.0, H 3.5, N 15.5; found: C 19.0, H 3.5, N 15.6.

[Pd(2,2′-bpy){Pt(*N1*-CH-*N3*)(en)(UH-*N1*)}$_2$](NO$_3$)(ClO$_4$)·4.9H$_2$O (2a): [$PdCl_2$(2,2′-bpy)] (13.3 mg, 39.4 μmol) was added to a solution of $AgClO_4{\cdot}H_2O$ (16.2 mg, 1.96 equiv) in H_2O (4 mL) and the suspension was stirred in the dark at 40 °C overnight. The resulting mixture was kept in an ice bath for 1 h and then the AgCl precipitate was centrifuged off. Subsequently, [Pt(en)(UH-*N1*)(CH$_2$-*N3*)]ClO$_4$·3H$_2$O (**1b**; 50.5 mg, 80.0 μmol) was added to the filtrate and the mixture was stirred for 1 day. The pH value was adjusted to 10 by means of NaOH (1 M) and a small amount of $NaNO_3$ was added to improve crystallization. The solution was kept at room temperature in a dish covered with parafilm. After three days, the mixture consisted of **1b** (40 %) and light-yellow crystals of **2a** (60 %), which were separated by hand under a microscope. Elemental analysis: calcd (%) for $C_{30}H_{38}N_{17}O_{13}ClPt_2Pd{\cdot}6H_2O$ (1484.8): C 24.2, H 3.4, N 16.0; found: C 24.1, H 3.5, N 16.2. X-ray analysis showed a slightly lower H_2O content.

[{Pd(2,2′-bpy)}$_3${Pt(en)(U-*N1*,*N3*,*O4*)(CH-*N1*,*N3*)}$_2$](NO$_3$)$_4$·5H$_2$O (4) and [{Pt(en)}$_2$(*N1*-U-*N3*,*O4*)$_2$(*N3*-CH-*N1*,*O2*)$_2${Pd(2,2′-bpy)}$_4$](NO$_3$)$_6$ (7): [$PdCl_2$(2,2′-bpy)] (302 mg, 0.901 mmol) was added to a solution of $AgNO_3$ (301 mg, 1.96 equiv) in H_2O (15 mL) and the suspension was stirred in the dark at 40 °C overnight. The resulting mixture was kept in an ice bath for 1 h before the AgCl precipitate was filtered off. Afterwards, [Pt(en)(UH-*N1*)(CH$_2$-*N3*)]ClO$_4$·3H$_2$O (**1b**; 283 mg, 0.448 mmol) was added to the filtrate and the mixture was stirred for 2 days. The pH value was adjusted to 7.5 by means of NaOH (1 M) and the solution was kept at 4 °C. After approximately two weeks, the solution was dry and a mixture of a small amount of orange blocks (**7**) and a large amount of a yellow precipitate was recovered. The orange crystals (**7**) were separated by hand under a microscope and turned out to be suitable for X-ray crystallography. The yellow precipitate was recrystallized from a 0.1 M KNO_3 solution and the pH value was adjusted to 9.5 by addition of NaOH (1 M). After 3 days at room temperature, crystals of **4** suitable for X-ray crystallography were obtained. Yield of **4**: 28 %; elemental analysis of **4**: calcd (%) for $C_{50}H_{52}N_{24}O_{18}Pt_2Pd_3{\cdot}8H_2O$ (2130.7): C 28.1, H 3.2, N 15.8; found: C 28.1, H 3.1, N 15.9.

[{Pt(en)(*N1*-U-*N3*)(*N3*-CH-*N1*)}$_4${Pd(2,2′-bpy)}$_4$](NO$_3$)$_3$(ClO$_4$)·56.1H$_2$O (9a): [$PdCl_2$(2,2′-bpy)] (102 mg, 0.303 mmol) was added to a solution of $AgNO_3$ (102 mg, 1.96 equiv) in H_2O (4 mL) and the suspension was stirred in the dark at 40 °C overnight. The resulting mixture was kept in an ice bath for 1 h before the AgCl precipitate was filtered off. Afterwards, [Pt(en)(UH-*N1*)(CH$_2$-*N3*)]ClO$_4$·3H$_2$O (**1b**; 189 mg, 0.300 mmol) was added to the filtrate and the mixture was stirred for 2 days. The pH value was adjusted to 10.5 by means of NaOH (1 M) and the solution was kept in a closed dish at 4 °C. After approximately four weeks, yellow crystals suitable for X-ray crystallography were obtained in low yield. Elemental analysis of the sample kept in air: calcd (%) for $C_{80}H_{88}N_{39}O_{25}ClPt_4Pd_4{\cdot}16H_2O$ (3525.5): C 27.2, H 3.4, N 15.5; found: C 27.1, H 3.1, N 15.5. Further concentration of the filtrate resulted in a precipitate which, according to ^{1}H NMR spectroscopy, consisted mostly of **4**.

[{Pt(en)}$_2$U$_2$(CH)$_2${Pd(en)}$_2$](NO$_3$)$_2$ (Y): [$PdCl_2$(en)] (20.2 mg, 85.1 μmol) was added to a solution of $AgNO_3$ (28.5 mg, 1.96 equiv) in H_2O (5 mL) and the suspension was stirred in the dark at 40 °C overnight. The resulting mixture was kept in an ice bath for 1 h before the AgCl precipitate was centrifuged off. Afterwards, [Pt(en)(UH-*N1*)(CH$_2$-*N3*)]NO$_3$·3.5H$_2$O (**1a**, 98.1 mg, 0.170 mmol) was added to the filtrate and the solution was stirred for 2 days. The pH value was adjusted to 7.4 by means of NaOH (1 M) and the solution was kept at room temperature. After 10 days, a mixture (40.3 mg) was recovered as a precipitate. According to ^{1}H NMR spectroscopy, the mixture consisted of **1a** (10 %) and **Y** (90 %). The mixture was characterized by ESI mass spectrometry.

[{Pt(en)(U-*N1*,*N3*,*O2*,*O4*)(C-*N1*,*N3*,*N4*,*O2*)}$_2${Pd(en)}$_6$](NO$_3$)$_5$-(ClO$_4$)$_3$·21.2H$_2$O (11′): [$PdCl_2$(en)] (213 mg, 0.898 mmol) was added to a solution of $AgNO_3$ (300.7 mg, 1.96 equiv) in H_2O (15 mL) and the suspension was stirred in the dark at 40 °C overnight. The resulting mixture was kept in an ice bath for 1 h before the AgCl precipitate was filtered off. [Pt(en)(UH-*N1*)(CH$_2$-*N3*)]ClO$_4$·3H$_2$O (**1b**, 284 mg, 0.450 mmol) was then added to the filtrate and the mixture was stirred for 2 days. The pH value was adjusted to 4.1 by means of NaOH (1 M) and the solution was kept at 4 °C in an open beaker. Within 7 days, orange cubes formed, which were filtered off, washed with a small amount of ice water, and dried in air. Yield: 35 %; elemental analysis of sample kept in air: calcd (%) for $C_{32}H_{74}N_{31}O_{33}Cl_3Pt_2Pd_6{\cdot}10H_2O$ (2736.3): C 14.1, H 3.4, N 15.8; found: C 14.1, H 3.6, N 15.7.

Characterization and physicochemical measurements: Elemental (C, H, N) analysis data were obtained on a Leco CHNS 932 instrument. ^{1}H NMR spectra in D_2O were recorded on Varian mercury 200 FT NMR and/or on Bruker DRX 400 instruments with sodium-3-(trimethylsilyl)-propanesulfonate (TSP, $\delta = 0$ ppm) or, for the host–guest studies, tetramethylammonium tetrafluoroborate (TMA, $\delta = 3.18$ ppm) as an internal reference. The ^{1}H,^{1}D-NOE, ^{1}H,^{1}D-TOCSY, and 2D (HSQC, HMBC) spectra were recorded on a Varian Inova 600 spectrometer with a 5 mm inverse detection probe with a *z*-gradient coil. All spectra were obtained by using pulse sequences from the Varian pulse-sequence library. The pD values of the NMR samples were determined by use of a glass electrode and addition of 0.4 units to the uncorrected pH meter reading (pH*). The pK_a values of **1** were estimated from plots of $\Delta\delta$ versus pH* values.

Electrospray mass spectrometry: The mass spectrometry experiments described above were performed with a Bruker APEX IV FTICR mass spectrometer equipped with a superconducting 7 Tesla magnet and an Apollo ESI source utilizing a nickel-coated glass capillary with a 0.5 mm inner diameter. This ESI source had three differential pumping stages. Ions were continuously generated from 150 μM solutions of the complexes in water/methanol (approximately 1:1) which were introduced into the source with a syringe pump (Cole Parmer Instruments, Series 74900) at flow rates of approximately 3 μL min^{-1}. Parameters were adjusted as follows: capillary voltage: −4.4 to −4.7 kV; endplate voltage: −4.0 to −4.3 kV; capexit voltage: 30–150 V; skimmer 1 voltage: 8–10 V; skimmer 2 voltage: 5–8 V; temperature of drying gas: 30–50 °C. The experiments were carried out with a nebulizer gas pressure of 20 psi and a drying gas pressure of 5 psi. The ions were accumulated in the instruments hexapole for different time spans to provide information about fast fragmentation processes. The ions were then introduced into the FTICR analyzer cell, which was operated at pressures below 10^{-10} mbar, and detected by a standard excitation and detection sequence. In the APEX IV instrument, the ICR cell is a cylindrical "infinity" cell with equipotential-line-segmented trapping plates. Such cells are primarily used to avoid *z* ejection of ions when exciting them before image current detection. For each measurement, 32–256 scans were averaged to improve the signal-to-noise ratio.

IR multiphoton dissociation (IRMPD) experiments were performed by mass-selection of the whole-isotope patterns of the ions of interest with correlated sweeps and by irradiating them with the IRMPD laser (10.5 μm, 25 W) for different time intervals. Due to the rather low intensities of some of the ions, up to 512 scans were required to obtain good signal-to-noise ratios.

X-ray data collection: Data collection for **1a**, **2a**, **4**, **7**, **9a**, and **11′** was carried out on an Enraf-Nonius Kappa CCD diffractometer by using graphite-monochromated $Mo_{K\alpha}$ radiation ($\lambda = 0.7169$ Å).[32] Data reduction and cell refinement were performed by using the programs DENZO and SCALEPACK[33a] or with the program EvalCCD.[33b,c] Reflections, which were partly measured on previous and following frames, were used to scale these frames to each other. Merging of redundant reflections in part eliminates absorption effects and also considers crystal decay if pres-

Table 7. Crystallographic data for compounds **1a**, **2a**, **4**, **7**, **9a**, and **11′**.

	1a	**2a**	**4**	**7**[b]	**9a**	**11′**
empirical formula	$C_{10}H_{23}N_8O_{9.5}Pt$	$C_{30}H_{48.13}ClN_{17}O_{18.06}PdPt_2$	$C_{50}H_{62}N_{24}O_{23}Pd_3Pt_2$	$C_{60}H_{60}N_{28}O_{24}Pd_4Pt_2$	$C_{80}H_{200.2}ClN_{39}O_{81.1}Pd_4Pt_4$	$C_{32}H_{116.40}Cl_3N_{31}O_{54.20}Pd_6Pt_2$
F_w	595.40	1457.80	2082.04	2001.08	4246.68	2938.09
crystal system	triclinic	triclinic	triclinic	triclinic	tetragonal	tetragonal
space group	$P\bar{1}$	$P\bar{1}$	$P\bar{1}$	$P\bar{1}$	$P4_2/n$	$I4_1/a$
a [Å]	10.226(2)	13.639(3)	12.270(2)	13.478(3)	41.132(6)	19.775(3)
b [Å]	12.792(3)	16.802(3)	13.385(3)	14.940(3)	41.132(6)	19.775(3)
c [Å]	15.027(3)	22.453(4)	21.199(4)	23.317(5)	23.372(5)	23.921(5)
α [°]	96.20(3)	79.32(3)	87.24(3)	79.12(3)	90.00	90.00
β [°]	91.20(3)	77.93(3)	75.76(3)	82.05(3)	90.00	90.00
γ [°]	94.13(3)	73.23(3)	80.87(3)	70.17(3)	90.00	90.00
V [Å^3]	1948.3(7)	4774.5(16)	3331.7(11)	4323.4(15)	39542(12)	9354(3)
Z	4	4	2	2	10	4
D_c [g cm^{-3}]	2.030	2.028	2.075	1.537	1.783	2.086
$\mu(Mo_{K\alpha})$ [mm^{-1}]	7.266	6.361	5.075	4.089	4.090	4.302
Gof on F^2	0.648	0.803	0.780	0.920	0.879	1.010
R_1, wR_2 $[I>2\sigma(I)]$[a]	0.0409, 0.0622	0.0496, 0.1058	0.0554, 0.0919	0.0577, 0.1130	0.0424, 0.0851	0.0484, 0.1296
R_1, wR_2 (all data)[a]	0.1242, 0.0771	0.1256, 0.1205	0.1553, 0.1093	0.1192, 0.1267	0.1102, 0.0968	0.0839, 0.1466

[a] $R_1=\Sigma||F_o|-|F_c||/\Sigma|F_o|$, $wR_2=[\Sigma w(F_o^2-F_c^2)^2/\Sigma w(F_o^2)^2]^{1/2}$. [b] Cation of **7** (solvent and counterion contribution eliminated from reflection data with the PLATON-SQUEEZE program).

ent. All of the structures were solved by standard Patterson methods[34a] and refined by full-matrix least-squares methods based on F^2 by using the SHELXTL-PLUS[34b] and SHELXL-97[34c] programs. Crystallographic data are compiled in Table 7. Owing to the large number of disordered counterions and/or disordered water molecules in the structure of **7**, the X-ray data for this compound were corrected by employing the SQUEEZE routine in the PLATON programme package.[35] 367 electrons were removed from a volume of 1519.2 Å^3, which were attributed to 12 NO_3^- counterions in the unit cell ($Z=2$). All atoms of the cation of **7** were refined anisotropically with the exception of two carbon atoms and one nitrogen atom of the en ligand, which were disordered over positions with 50% occupancies in each.

In **9a**, of the five anions required per asymmetric unit, 1.2 have been refined as ClO_4^- (spread over 3 positions, with 1 of these being a center of inversion generating a fully occupied ClO_4^- in the packing) and 3.8 as NO_3^- (distributed over 11 positions). Two of these nitrate ions, defined by N(4N), O(41N), O(42N), and O(43N), as well as O(42N), N(4N), O(44N), and O(45N), share the same space with 25% occupancy each, in such a way that O(42N) defines the position of an oxygen atom in one nitrate ion while it defines the position of the central nitrogen atom in the second. The same but the other way around is true for N(4N). 70.1 water molecules per asymmetric unit occupy 117 positions, with some of them shared with only partially occupied anions. The occupancy of the water molecules was refined by allowing a maximum of 0.15 for the thermal displacement factors. All atoms of the cations were refined anisotropically with the exception of one C4 atom of one of the cytosine bases (non-positive defined). Anisotropic refinement was further applied to the ClO_4^- anion on the special position as well as to all fully occupied water molecules.

With **11′**, per asymmetric unit, one nitrate anion with the nitrogen atom on a center of inversion as well as another nitrate and a perchlorate anion, both with only 75% occupancy, could be refined. The oxygen atoms of all anions are disordered over multiple positions. The same is true for the 5.3 water molecules found per asymmetric unit. The occupancy of these water molecules was refined freely assuming thermal displacement factors similar to those found for the oxygen atoms of the anions ($\approx$0.15–$\approx$0.2), with the exception of positions with restricted occupancies due to disorder with other water molecules and/or anions. 4.45 water molecules are distributed over 14 positions with occupancies ranging from 10–50%. The remaining positions are shared with partially occupied oxygen atoms of the anions. All atoms of the cation were refined anisotropically with the exception of one carbon atom of each en ligand, each of which was disordered over two positions, all with occupancies of 50%.

CCDC-623 122–623 127 contain the supplementary crystallographic data for this paper. These data can be obtained free of charge from the Cambridge Crystallographic Data Centre via www.ccdc.cam.ac.uk/data_request/cif.

Acknowledgement

This work was supported by the Deutsche Forschungsgemeinschaft (DFG) and the Fonds der Chemischen Industrie (FCI). We thank Mrs M. Morell Cerdà for her help in collecting the X-ray data for some of the compounds.

[1] H. Rauter, E. C. Hillgeris, A. Erxleben, B. Lippert, *J. Am. Chem. Soc.* **1994**, *116*, 616–624.
[2] H. Rauter, E. C. Hillgeris, B. Lippert, *J. Chem. Soc. Chem. Commun.* **1992**, 1385–1386.
[3] Reviews: a) J. A. R. Navarro, E. Barea, M. A. Galindo, J. M. Salas, M. A. Romero, M. Quirós, N. Masciocchi, S. Galli, A. Sironi, B. Lippert, *J. Solid State Chem.* **2005**, *178*, 2436–2451; b) J. A. R. Navarro, B. Lippert, *Coord. Chem. Rev.* **2001**, 219–250.
[4] J. A. R. Navarro, M. B. L. Janik, E. Freisinger, B. Lippert, *Inorg. Chem.* **1999**, *38*, 426–432.
[5] a) H. Rauter, I. Mutikainen, M. Blomberg, C. J. L. Lock, R. Amo-Ochoa, E. Freisinger, L. Randaccio, E. Zangrando, E. Chiarparin, B. Lippert, *Angew. Chem.* **1997**, *109*, 1353–1357; *Angew. Chem. Int. Ed. Engl.* **1997**, *36*, 1296–1301; b) J. A. R. Navarro, E. Freisinger, B. Lippert, *Eur. J. Inorg. Chem.* **2000**, 147–151; c) J. A. R. Navarro, J. M. Salas, *Chem. Commun.* **2000**, 235–236; d) J. A. R. Navarro, E. Freisinger, B. Lippert, *Inorg. Chem.* **2000**, *39*, 2301–2305.
[6] Z. Qin, M. C. Jennings, R. J. Puddephatt, *Inorg. Chem.* **2002**, *41*, 3967–3974.
[7] E. Barea, J. A. R. Navarro, J. M. Salas, M. Quirós, M. Willermann, B. Lippert, *Chem. Eur. J.* **2003**, *9*, 4414–4421.

[8] M. A. Galindo, S. Galli, J. A. R. Navarro, M. A. Romero, *Dalton Trans.* **2004**, 2780–2785.
[9] L. C. Tabares, J. A. R. Navarro, J. M. Salas, *J. Am. Chem. Soc.* **2001**, *123*, 383–387.
[10] J. A. R. Navarro, E. Freisinger, B. Lippert, *Eur. J. Inorg. Chem.* **2000**, 147–151.
[11] M. J. Rauterkus, B. Krebs, *Angew. Chem.* **2004**, *116*, 1321–1324; *Angew. Chem. Int. Ed.* **2004**, *43*, 1300–1303.
[12] The authors of reference [11] have not made any detailed proposal concerning the method of formation of their Pt_5 compounds. However, the latter can be considered as being formed from an initial Pt_3 cycle.
[13] Reviews: a) B. Lippert, *Prog. Inorg. Chem.* **1989**, *37*, 1–97; b) B. Lippert, *Coord. Chem. Rev.* **1999**, *182*, 263–295.
[14] B. Lippert in *Cisplatin-Chemistry and Biochemistry of a Leading Anticancer Drug* (Ed: B. Lippert), Wiley-VCH, Weinheim, **1999**, pp. 379–403.
[15] a) K. Matsumoto, K. Sakai, *Adv. Inorg. Chem.* **2000**, *49*, 375–427; b) K. Sakai, Y. Tanaka, Y. Tsachiya, K. Hirata, T. Tsubomura, S. Iijima, A. Bhattacharjee, *J. Am. Chem. Soc.* **1998**, *120*, 8366–8379.
[16] B. Lippert, *Inorg. Chem.* **1981**, *20*, 4326–4343.
[17] For examples of dynamic combinatorial libraries containing metal ions see: a) J.-M. Lehn, *Chem. Eur. J.* **1999**, *5*, 2455–2463; b) E. Stulz, S. M. Scott, A. D. Bond, S. J. Teat, J. K. M. Sanders, *Chem. Eur. J.* **2003**, *9*, 6039–6048; c) S. Gauthier, L. Quebatte, R. Scopelliti, K. Severin, *Chem. Eur. J.* **2004**, *10*, 2811–2821; d) I. Saur, R. Scopelliti, K. Severin, *Chem. Eur. J.* **2006**, *12*, 1058–1066; e) T. Brasey, R. Scopelliti, K. Severin, *Inorg. Chem.* **2005**, *44*, 160–162; f) Y. Kubota, S. Sakamoto, K. Yamaguchi, M. Fujita, *Proc. Natl. Acad. Sci. USA* **2002**, *99*, 4854–4856.
[18] a) L. Clowney, S. C. Jain, A. R. Srinivasan, J. Westbrook, W. K. Olson, H. M. Berman, *J. Am. Chem. Soc.* **1996**, *118*, 509–518, and references therein; b) R. Taylor, O. Kennard, *J. Mol. Struct.* **1982**, *78*, 1–28, and references therein.
[19] R. Faggiani, B. Lippert, C. J. L. Lock, *Inorg. Chem.* **1980**, *19*, 295–300.
[20] a) W. Brüning, E. Freisinger, M. Sabat, R. K. O. Sigel, B. Lippert, *Chem. Eur. J.* **2002**, *8*, 4681–4692; b) W. Brüning, I. Ascaso, E. Freisinger, M. Sabat, B. Lippert, *Inorg. Chim. Acta* **2002**, *339*, 400–410; c) S. Jaworski, H. Schöllhorn, P. Eisenmann, U. Thewalt, B. Lippert, *Inorg. Chim. Acta* **1988**, *153*, 31–38.
[21] W. Brüning, PhD Thesis, University of Dortmund (Germany), **1997**.
[22] See for example: a) B. Lippert, R. Pfab, D. Neugebauer, *Inorg. Chem. Acta*, **1979**, *37*, L495–L497; b) M. Ruf, K. Weis, H. Vahrenkamp, *Inorg. Chem.* **1997**, *36*, 2130–2137.
[23] J. J. Christen, J. H. Rytting, R. M. Izatt, *J. Phys. Chem.* **1967**, *71*, 2700–2705.
[24] a) R. J. De Pasquale, *Ind. Eng. Chem. Prod. Res. Dev.* **1978**, *17*, 278–286; b) S. Ganguly, K. K. Kundu, *Can. J. Chem.* **1994**, *72*, 1120–1126; c) J. R. DeMember, F. A. Wallace, *J. Am. Chem. Soc.* **1975**, *97*, 6240–6245.
[25] W. Micklitz, W. S. Sheldrick, B. Lippert, *Inorg. Chem.* **1990**, *29*, 211–216.
[26] E. Pretsch, P. Bühlmann, C. Affolter, *Structure Determination of Organic Compounds*, Springer, Berlin, **2000**.
[27] K. S. Jeong, S. Y. Kim, U.-S. Shin, T. M. H. Nguyen, M. Kogej, P. Broekmann, N. Jeong, B. Kirchner, M. Reiher, C. A. Schalley, *J. Am. Chem. Soc.* **2005**, *127*, 17672–17685.
[28] a) C. A. Schalley, T. Müller, P. Linnartz, M. Witt, M. Schäfer, A. Lützen, *Chem. Eur. J.* **2002**, *8*, 3538–3551; b) M. Engeser, A. Rang, M. Ferrer, A. Gutiérrez, H. T. Baytekin, C. A. Schalley, *Int. J. Mass Spectrom.* **2006**, *255–256*, 185–194.
[29] For reviews highlighting the utility of mass spectrometry for the study of noncovalent compounds see: a) C. A. Schalley, *Mass Spectrom. Rev.* **2001**, *20*, 253–309; b) B. Baytekin, H. T. Baytekin, C. A. Schalley, *Org. Biomol. Chem.* **2006**, *4*, 2825–2841.
[30] F. Basalo, J. C. Bailar, B. R. Tarr, *J. Am. Chem. Soc.* **1950**, *72*, 2433–2438.
[31] B. J. McCormick, E. N. Jaynes, Jr., R. I. Kaplan, *Inorg. Synth.* **1972**, *13*, 216–218.
[32] Kappa CCD package, Nonius, Delft (The Netherlands), **1997**.
[33] a) DENZO and SCALEPACK: Z. Otwinowsky, W. Minor, *Methods Enzymol.* **1997**, *276*, 307–326; b) EvalCCD, Brucker-AXS Inc., Madison, WI (USA), **2002**; c) A. J. M. Duisenberg, L. M. J. Kroon-Batenburg, A. M. M. Schreurs, *J. Appl. Crystallogr.* **2003**, *36*, 220–229.
[34] a) G. M. Sheldrick, *Acta Crystallogr. Sect. A* **1990**, *46*, 467–473; b) SHELXTL-PLUS (VMS), G. M. Sheldrick, Madison, WI (USA), **1990**; c) SHELX-97, Program for Crystal Structure Refinement, G. M. Sheldrick, University of Göttingen (Germany), **1997**.
[35] A. L. Spek, *Acta Crystallogr. Sect. A* **1990**, *46*, C34.

Received: October 27, 2006
Published online: April 30, 2007

